

DUST IN THE SMALL MAGELLANIC CLOUD: INTERSTELLAR POLARIZATION AND EXTINCTION

C. V. RODRIGUES¹ AND A. M. MAGALHÃES^{2,3,4,5}

Instituto Astronômico e Geofísico, Universidade de São Paulo, Caixa Postal 9638, São Paulo, SP 01065-970, Brazil;
claudia@das.inpe.br, mario@argus.iagusp.usp.br

G. V. COYNE, S.J.

Specola Vaticana, Vatican Observatory, V-00120 Vatican City State, Rome, Italy; gcoyne@as.arizona.edu

AND

V. PIROLA

Tuorla Observatory, Turku University, Väisäläntie 20 FIN-21500, Piikkiö, Finland; pirola@sara.cc.utu.fi

Received 1995 December 7; accepted 1997 March 24

ABSTRACT

The typical extinction curve for the Small Magellanic Cloud (SMC), in contrast to that for the Galaxy, has no bump at 2175 Å and a steeper rise into the far-ultraviolet. For the Galaxy, the interpretation of the extinction, and therefore the dust content of the interstellar medium, has been greatly assisted by measurements of the wavelength dependence of the polarization. Up to the present, no such measurements existed for the SMC.

Therefore, to further elucidate the dust properties in the SMC, we have measured, for the first time, linear polarization in five colors in the optical region of the spectrum for a sample of reddened stars. For two of these stars, for which there were no existing UV spectrophotometric measurements, but for which we measured a relatively large polarization, we have also obtained data from the *IUE* in order to study the extinction. With the help of parameterization, we attempted to correlate the SMC extinction and polarization data. In addition, we performed dust model fits to both extinction and polarization using silicate and graphite, or amorphous carbon spheres and silicate cylinders. The size distribution for the cylinders is taken from a fit to the polarization, and we introduce the notion of volume continuity between this and the silicate sphere size distribution.

The main results are (1) the wavelength of maximum polarization, λ_{\max} , in the SMC is typically smaller than that in the Galaxy; (2) however, AZV 456, which shows the UV extinction bump, has a λ_{\max} typical of that in the Galaxy, its polarization curve is narrower, its bump is shifted to shorter wavelengths as compared with the Galaxy, and its UV extinction does not conform to the Galactic analytical interpolation curve based on the ratio of total to selective extinction; (3) the “typical,” monotonic SMC extinction curve can be best fitted with amorphous carbon and silicate grains; (4) the extinction toward AZV 456 may be explained only by assuming a larger gas-to-dust ratio than the observed $N(\text{H I})/A(V)$ value, with a small amount of the available carbon in graphite form; and (5) from an analysis of both the extinction and polarization data and our model fits, it appears that the SMC has typically smaller grains than those in the Galaxy.

The absence of the extinction bump in the SMC generally has been thought to imply a lower amount or even an absence of carbon in solid form in the SMC compared with the Galaxy. Our results show that the size distribution, and not only the carbon abundance, is different in the SMC as compared with the Galaxy. In addition, and contrary to previous findings, another component besides silicates is indeed needed to provide a sizable part of the observed extinction toward the SMC. Using the SMC as a laboratory for studying the solid component of the interstellar medium, we also discuss some of the implications of our results in view of proposed interstellar dust models.

Subject headings: dust, extinction — Magellanic Clouds — polarization — ultraviolet: ISM

1. INTRODUCTION

The interstellar medium (ISM) in galaxies is indicative of their evolutionary state and of their stellar populations. For instance, the Galaxy contains 4 times more heavy elements

than the Large Magellanic Cloud (LMC) and 10 times more than the Small Magellanic Cloud (SMC) (Wheeler, Sneden, & Truran 1989). The dust content of the ISM in the LMC (Koorneef 1982; Fitzpatrick 1985a) and the SMC (Bouchet et al. 1985; Fitzpatrick 1985b) is less than in the Galaxy, and the dust is qualitatively different. In particular, the SMC has a steeper far-ultraviolet (FUV) extinction curve (Prévot et al. 1984); it typically has no ultraviolet (UV) extinction bump. The SMC also has a weak infrared (IR) emission at 12 μm and an intensity ratio 60 $\mu\text{m}/100 \mu\text{m}$ larger than that in the Galaxy (Lequeux 1989). This would appear to indicate that star formation and evolution have proceeded at a faster rate in the Galaxy than in the LMC or the SMC, and/or that dust grains have formed there differ-

¹ Now at Instituto Nacional de Pesquisas Espaciais-INPE, Divisão de Astrofísica-DAS, Caixa Postal 515, São José dos Campos, SP 12201-970, Brazil.

² Guest observer at *IUE*.

³ Visiting Astronomer, Cerro Tololo Inter-American Observatory, which is operated by AURA, Inc., under contract to the National Science Foundation.

⁴ Visiting Astronomer, Complejo Astronómico El Leoncito, San Juan, Argentina.

⁵ Visiting Astronomer, European Southern Observatory, La Silla, Chile.

ently in a different environment. In fact, there is some indication that the efficiency of grain formation in the LMC and the SMC may be slightly lower, albeit similar, compared with that in the Galaxy (Clayton & Martin 1985). Also, from data on M31, it is suggested that the abundance of small grains may be related to star formation rates (Xu & Helou 1994).

For these reasons, and because of its proximity, the SMC is an important environment in which to study dust grains. Dust may cause several observable effects: it attenuates, reddens, scatters, and polarizes starlight; it absorbs and reemits radiation; and it may bring about a depletion of the gas content of the ISM and may serve as a catalyst for the formation of molecules in the ISM. In the case of the SMC, the higher FUV radiation field, together with the lower dust content, produces an increased photodissociation of molecules that affects the properties of molecular clouds (Lequeux et al. 1994). The SMC is thus an excellent laboratory to study dust in an environment quite distinct from that of the Galaxy, while at the same time allowing us to test dust models that have been proposed. We concentrate our study on the reddening and the polarization due to dust in the SMC.

It has been known for some time from *IUE* observations that the UV and FUV extinction relative to the visual and the IR is much larger in both the LMC (Nandy et al. 1981; Koorneef & Code 1981; Fitzpatrick 1985a, 1986) and the SMC (Prévot et al. 1984) than it is in the Galaxy, and the effect is larger for the SMC than it is for the LMC. The SMC is also noteworthy for the lack of the extinction bump at 2175 Å (see review by Fitzpatrick 1989). Interstellar polarization in connection with extinction in the LMC context has been studied by Clayton, Martin, & Thomson (1983), Clayton & Martin (1985), and Clayton et al. (1997).

Interestingly, the SMC star AZV 456 (AZV = Azzopardi & Vigneau 1982) shows an extinction and a gas-to-dust ratio (Lequeux et al. 1984) similar to the average values in the Galaxy. The interstellar lines in this direction have typical velocities for the SMC, so that the extinction is probably not foreground (Lequeux et al. 1984; Martin, Maurice, & Lequeux 1989). There is an IR extended source in the SMC located at the same coordinates as AZV 456 (LI-SMC 190; Schwering & Israel 1989), which also indicates that the extinction is within the SMC. Lequeux (1994) has raised the possibility that AZV 456 may have, in fact, a higher gas-to-dust ratio due to a possibly undetected amount of H₂. In § 5.3.2, we show that such a higher ratio is indeed required if the extinction toward this object is fitted appropriately.

Classical models for fitting the wavelength dependence of the extinction by dust grains in the ISM of galaxies generally take into account the chemical composition of the grains and their size distribution. Bromage & Nandy (1983) and Pei (1992) studied the SMC “typical” extinction curve using the model of Mathis, Rumpl, & Nordesiek 1977 (hereafter MRN) with only spherical particles. They concluded that, by simply lowering the quantity of graphite grains relative to silicates in the Galactic models, it was possible to fit the *wavelength dependence* of the SMC extinction without changes in the sizes used to obtain the Galactic curve. Pei (1992) and Maccioni & Perinotto (1994) have studied the extinction in the LMC, and the latter noted from their fits to the extinction that no unique solution could be obtained for the grain sizes and abundance ratios.

In the Galaxy, it is known that the wavelength at which the polarization is maximum is related to the grain size (Coyne, Gehrels, & Serkowski 1974). Therefore, it would be very useful to have this information for the SMC. No wavelength-dependent polarization measurements have been published yet on the SMC. In this paper, we present the first such observations and analyze them in light of the extinction, for which we also report a few new *IUE* observations. In addition, we present some model fits to these observations.

2. DATA

2.1. Polarization Data

2.1.1. Observations

Polarimetric observations have been obtained during several observing runs at various observatories and with various polarimeters. The observing runs were as follows: 1983 with the MINIPOL polarimeter (Frecker & Serkowski 1976) on the 1.5 m telescope at the Cerro Tololo Inter-American Observatory, 1987 with the PISCO polarimeter (Stahl et al. 1986) on the 2.2 m telescope of the European Southern Observatory (ESO), and 1986, 1988 October, 1988 November, and 1989 with the VATPOL polarimeter (Magalhães, Benedetti, & Roland 1984) on the 2.15 m telescope at the Complejo Astronómico El Leoncito (CASLEO). About 70% of the observations were made at CASLEO.

VATPOL and MINIPOL provide on-line data reduction after each integration and/or after a series of integrations (the integration time can be freely selected). This data reduction consists of a least-squares fit to a double cosine curve of the counts from two photomultiplier tubes obtained as a function of the position of a rotating half-wave plate. The mean error of the polarization is calculated from the actual deviations of the two counts from the double cosine curve; this error is consistent typically with photon-noise error, as detailed by Magalhães et al. (1984). The data from PISCO were obtained in FITS format, and we wrote a special microcomputer program to calculate the polarization from the star and sky counts in a way similar to that of the other two instruments.

All data have been corrected for instrumental effects and standardized. Unpolarized standard stars were measured to obtain corrections for instrumental polarization. Nightly measurements were made on highly polarized standard stars and also with a Glan-Air prism in the beam in order to obtain the polarizing efficiencies and to standardize the polarization position angles to the equatorial system. The polarizing efficiencies were typically 98%–99% for VATPOL and MINIPOL. For the measurements with PISCO, the efficiencies were provided to us by H. Schwarz of ESO. Repeated runs at CASLEO showed all corrections measured there to be stable. Corrections for bias in the linear polarization, which depend on the ratio of the error to the percentage polarization (Clarke & Stewart 1986), were also applied. We note, however, that all calculations were made using the Stokes parameters.

We combine the results from the three instrumental systems in the following way. For each star, we first calculate the weighted average of the measurements made with each filter in each of the instrumental systems. We then determine the weighted mean of those averages. The results, both observed and corrected for foreground polarization

(see § 2.1.2), are given in Table 1, where the respective columns are as follows: (1) star number from Azzopardi & Vigneanu (1982, hereafter AZV82); (2) star number from Sanduleak (1968, 1969); (3)–(5) the observed polarization (equal to the weighted mean polarization over the averages obtained from each observing run), the standard deviation of the mean, and the polarization position angle in the equatorial system, respectively; (6)–(8) same as columns (3)–(5), but for the foreground-corrected polarization; and (9) the effective wavelength (averaged over the values for each observing run, by weighting with the mean polarization errors). The foreground-corrected polarization measurements are plotted in Figure 1.

The targets reported in Table 1 have been selected for multifilter polarimetry from our ongoing program to map the magnetic field structure of the SMC (Magalhães et al. 1990). The sample was built from the AZV82 catalog, avoiding stars with emission-line spectra. Presently, this survey is being conducted with CCD imaging polarimetry (Magalhães et al. 1996), and the results will be reported elsewhere.

2.1.2. Foreground Polarization Corrections

It is necessary to correct the measured polarizations by subtracting the polarization foreground to the SMC due to dust in the Galaxy. It is expected that these corrections are important, since the interstellar reddening intrinsic to the SMC is small. We have selected published, unfiltered polar-

ization data (Mathewson & Ford 1970; Schmidt 1976) on about 40 stars farther than 400 pc from the Sun in the direction of the stars measured in the SMC. McNamara & Feltz (1980) have shown that most of the foreground extinction to the SMC occurs within 400 pc from the Sun. Also by this selection, we include most of the dust in the Galactic plane for which the scale height is 120 pc (Burton et al. 1986).

As a check on this procedure, we also have estimated the foreground polarization in two additional ways. The first way was to average the polarization data of our survey sample (Magalhães et al. 1990; Rodrigues 1992) for stars in the SMC that showed an observed polarization equal to or less than 0.4%. We also averaged polarization data, again using data from our survey, for SMC stars having an estimated color excess less than 0.09 mag. This upper limit for the foreground reddening toward the SMC is suggested by Schwering (1988); McNamara & Feltz (1980) and Bessel (1991) have suggested lower values (0.02 mag and 0.04–0.06 mag, respectively). We have estimated the color excess for the SMC stars in our sample using the intrinsic colors from Fitzgerald (1970) and Brunet (1975). Both of these methods gave results that were entirely consistent with the estimates from the Galactic foreground objects (Table 2) described in the previous paragraph, which we used for correcting the SMC data.

Table 2 gives the adopted corrections for the foreground polarization toward the various regions in the SMC defined

TABLE 1
SMC POLARIZATION DATA

IDENTIFICATION		OBSERVED			CORRECTED			
AZV	SK	P	σ_p	θ_p	P	σ_p	θ_p	λ_{eff}
(1)	(2)	(%)	(%)	(deg)	(%)	(%)	(deg)	(μm)
		(3)	(4)	(5)	(6)	(7)	(8)	(9)
126	...	1.149	0.095	107.5	0.737	0.126	104.1	0.379
		1.175	0.055	109.3	0.725	0.105	106.6	0.439
		1.076	0.040	111.4	0.598	0.102	109.7	0.559
		0.781	0.078	110.1	0.325	0.129	105.3	0.664
		0.825	0.083	108.6	0.407	0.120	103.7	0.791
211	74	1.207	0.044	126.6	0.943	0.085	127.3	0.378
		1.243	0.027	124.8	0.955	0.083	125.0	0.438
		1.250	0.075	126.0	0.947	0.112	126.6	0.516
		1.175	0.017	126.1	0.873	0.085	126.8	0.559
		1.063	0.018	127.6	0.774	0.082	128.9	0.664
		0.986	0.042	131.1	0.728	0.085	133.7	0.790
		0.991	0.080	125.0	0.726	0.107	125.3	0.820
215	76	0.782	0.035	148.5	0.626	0.086	158.3	0.437
		0.907	0.032	148.6	0.741	0.089	157.4	0.557
		0.742	0.033	148.5	0.587	0.087	159.2	0.662
		0.653	0.060	148.7	0.512	0.095	160.0	0.791
221	77	1.125	0.099	138.3	0.903	0.129	148.4	0.377
		1.048	0.047	140.9	0.862	0.101	153.3	0.437
		1.014	0.042	141.5	0.838	0.103	155.2	0.558
		0.799	0.060	144.3	0.698	0.109	161.6	0.663
		0.659	0.084	143.0	0.557	0.119	162.5	0.791
398	...	2.114	0.108	131.4	1.856	0.130	132.5	0.380
		2.084	0.058	132.5	1.810	0.098	133.8	0.440
		2.038	0.042	131.9	1.751	0.093	133.2	0.560
		1.948	0.058	134.6	1.679	0.099	136.4	0.665
		1.464	0.072	134.8	1.218	0.103	137.0	0.791
456	143	0.959	0.074	163.9	0.842	0.086	167.0	0.376
		1.147	0.060	160.0	1.006	0.076	162.3	0.437
		1.323	0.172	156.7	1.156	0.179	158.4	0.516
		1.338	0.045	160.9	1.195	0.067	163.0	0.559
		1.259	0.050	160.7	1.120	0.069	162.9	0.671
		1.133	0.059	161.3	1.006	0.073	163.6	0.791
		0.950	0.089	163.2	0.830	0.099	166.2	0.820

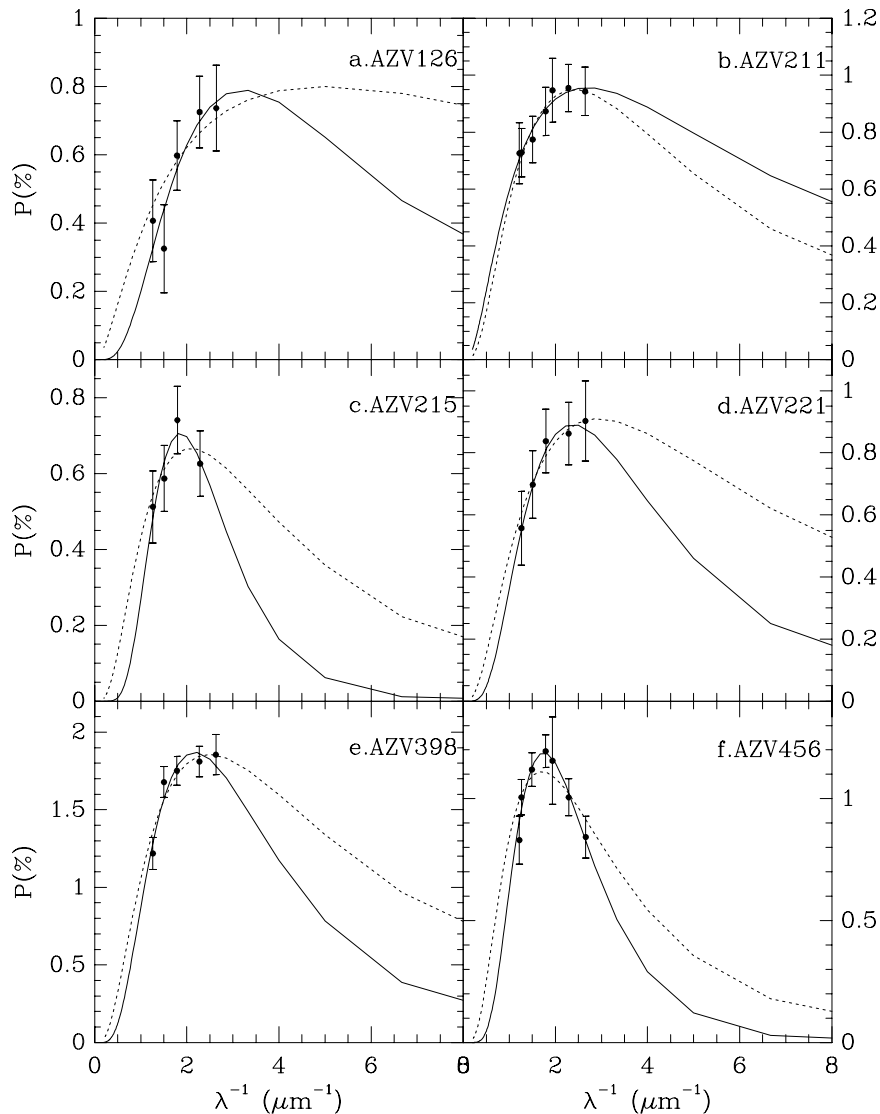


FIG. 1.—Polarization for the SMC stars. The points with error bars represent our foreground-corrected data. The solid lines and dotted lines show the three- and two-parameter Serkowski fits, respectively.

by Schmidt (1976). Our program stars are located as follows: region I, AZV 20, 126, and 221; region II, AZV 211, 215, and 398; and region III, AZV 456. The estimated values for the foreground polarization were taken as valid for the V filter. We used the Serkowski law, with $\lambda_{\max} = 0.55 \mu\text{m}$, to estimate the contribution in the other filters. The errors of the corrected polarization values include the increase in uncertainty arising from this correction. These are the values in Table 1. We tested the influence of changes

in λ_{\max} on the above estimates and on the resulting corrected data and found them to be insignificant.

2.2. UV Spectroscopic Data

Our UV sample consisted of three reddened stars, AZV 20, AZV 126, and AZV 211, and comparison stars necessary to obtain the extinction curves (see § 2.2.2). AZV 211 was our primary target because it had shown a well-determined polarization curve with a small λ_{\max} (Fig. 1 and Table 3). In our reduction, we have included the data already published on AZV 398 (Prévot et al. 1984) and on AZV 456 (Lequeux et al. 1984) in order to test our procedure and to give homogeneity to the sample studied in the following sections. The relevant data on the reddened stars and on the comparison stars are given in Tables 4 and 5, respectively.

The UV spectral data were obtained with the *IUE* (Boggess et al. 1978a, 1978b; Kondo 1987) in two runs: 1990 November and 1991 September. The images were obtained with three cameras: the short-wavelength prime (SWP; 1200–2000 Å), the long-wavelength prime (LWP; 2000–3200 Å), and the long-wavelength redundant (LWR; 2000–3200 Å). We have used some images from the *IUE*

TABLE 2

FOREGROUND POLARIZATION CORRECTIONS FOR VARIOUS REGIONS IN THE SMC

Region	P (%)	σ_P (%)	θ (deg)	σ_θ (deg)	N
I.....	0.47	0.09	113.6	14.0	6
II.....	0.30	0.08	124.1	8.0	10
III.....	0.17	0.05	145.0	8.2	11
IV.....	0.22	0.05	124.2	6.5	6
V.....	0.27	0.05	95.6	5.5	11

TABLE 3
PARAMETERS OF THE SERKOWSKI CURVE FROM FITS OF THE SMC POLARIZATION DATA

Star (1)	λ_{\max} (μm) (2)	$\sigma_{\lambda_{\max}}$ (μm) (3)	K (4)	σ_K (5)	P_{\max} (%) (6)	$\sigma_{P_{\max}}$ (%) (7)	χ^2_v (8)	$P(\chi^2_v)$ (9)	v (10)
AZV 126.....	0.31	0.31	1.0	1.8	0.79	0.34	0.73	0.48	2
	0.20	0.99	0.3	1.6	0.8	1.4	0.77	0.51	3
AZV 211.....	0.37	0.22	0.48	0.67	0.956	0.089	0.11	0.98	4
	0.42	0.06	0.70	0.10	0.950	0.053	0.11	0.99	5
AZV 215.....	0.54	0.05	2.5	1.9	0.707	0.071	0.54	0.46	1
	0.48	0.12	0.81	0.20	0.666	0.061	0.66	0.52	2
AZV 221.....	0.42	0.12	1.2	1.3	0.892	0.073	0.09	0.91	2
	0.34	0.14	0.57	0.23	0.910	0.140	0.13	0.94	3
AZV 398.....	0.46	0.04	1.26	0.55	1.87	0.07	1.15	0.32	2
	0.40	0.05	0.68	0.08	1.86	0.08	1.17	0.32	3
AZV 456.....	0.57	0.02	2.06	0.53	1.19	0.05	0.30	0.88	4
	0.59	0.03	0.98	0.06	1.11	0.03	1.10	0.36	5

data archive also (see last column of Tables 4 and 5). The images are unidimensional vectors with a sampling of 1 Å.

2.2.1. Obtaining the Combined Spectrum of Each Star

Each star has been observed, sometimes more than once, in each of the two wavelength ranges. The reductions were made using the RDAF and IUEIDL packages at the University of Wisconsin-Madison. The first procedure in the data reduction is to combine all the images of a star into one spectrum. Corrections for the time degradation of the camera sensitivity (Bohlin & Grillmair 1988a, 1988b) are made first. At the time this reduction was done, only corrections up to 1988 were available, so to correct the data obtained after that time, we had to use an extrapolation. Also, the cameras do not have the same efficiencies, so there may be a discontinuity in the overlap region between two spectra. Generally, it is assumed that the two spectra must have the same flux in the overlap region. Since we are interested only in the ratio between spectra of the program and the comparison stars (see eq. [1]), we have not corrected for this effect. The combined spectra did not in fact present any discontinuities.

2.2.2. Determination of Extinction Curves

We have obtained the extinction curves by using the pair method (Fitzpatrick & Massa 1986), which consists in com-

paring two stars of the same spectral type but with different reddening. The assumption is that the program and comparison stars have exactly the same intrinsic spectra, the observed difference being due to the foreground interstellar medium. We estimated the error in this assumption by using different comparison stars.

From the B and V magnitudes and the fluxes, ϕ_i , the normalized extinction is given by

$$\frac{E(\lambda - V)}{E(B - V)} = \frac{2.5 \log(\phi_c/\phi_r) - V_r + V_c}{(B - V)_r - (B - V)_c}, \quad (1)$$

where the subscripts r and c mean *reddened* and *comparison star*, respectively. Great care has been exercised in selecting appropriate comparison stars, especially for AZV 211 because of its relatively late spectral type. The comparison stars have been chosen from among SMC stars only, using the AZV82 catalog and excluding emission-line stars, which are often variable and present anomalous color excesses due to circumstellar material. We also chose these unreddened stars within a spectral subclass from AZV 211 with the purpose of matching as best we could this star's spectral type. Furthermore, we chose to stay with comparison objects within about 1 mag of AZV 211. By using SMC stars, we also minimize the effect of metallicity differences between comparison stars and reddened stars, since two

TABLE 4
RELEVANT DATA ON THE REDDENED STARS

Star (1)	Spectral Type (2)	$(B - V)_0^a$ (3)	V^b (4)	$(B - V)$ (5)	$(U - B)$ (6)	$E(B - V)$ (7)	IUE Images (8)
AZV 20.....	A0 Ia ^c	-0.04	12.1	+0.29	-0.12	+0.33	LWP 21313, 14, 15 SWP 42509, 39, 40
AZV 126.....	B0 Iw ^d	-0.25	13.47	-0.02	-0.90	+0.23	LWP 21279, 80 LWR 14947
AZV 211.....	A0 Ia ^e	-0.04	11.5	+0.10	-0.45	+0.14	SWP 42506, 18908 LWP 21279, 80 LWR 14947
AZV 398.....	B2 ^f	-0.18	13.85	+0.09	-0.77	+0.27	SWP 42506, 18908 LWR 14963
AZV 456.....	B0-1 ^f	-0.25	12.89	+0.10	-0.74	+0.37 ^g	SWP 18911 LWR 12347
						+0.35	SWP 16051
						+0.36 ^g	

^a Brunet 1975.
^b Photometry from AZV82.
^c Humphreys 1983.
^d Garmany, Conti, & Massey 1987.
^e Ardeberg et al. 1972.
^f Prévot et al. 1984.
^g Bouchet et al. 1985.

TABLE 5
RELEVANT DATA ON THE COMPARISON STARS

Comparison Star	Reddened Star	Spectral Type	$(B-V)_0^a$	V^b	$(B-V)$	$(U-B)$	<i>IUE</i> Images
AZV 61	AZV 126	O5 V ^c	+0.01	13.68	-0.23	-0.98	LWP 19245
AZV 161	AZV 20	A0 I ^d	+0.01	11.80	+0.03	-0.40	LWP 19245
	AZV 211						SWP 40139
AZV 235	AZV 398	B0 Iw ^e	-0.24	12.15	-0.12	-0.94	LWR 7239, 84
	AZV 456						SWP 8293
AZV 242	AZV 398	B1 I ^d	-0.19	12.08	-0.10	-0.88	LWR 7242
	AZV 456						SWP 8296
AZV 270	AZV 20	A0 Ia ^f	+0.02	11.43	+0.03	-0.42	LWP 19241, 44
	AZV 211						SWP 40134, 37
AZV 289	AZV 398	B0.5 I ^c	-0.22	12.42	-0.14	-0.94	LWR 12345
	AZV 456						SWP 16049, 18829
AZV 317	AZV 126	B0 Iw ^e	-0.24	12.90	-0.20	-1.00	LWR 17264
	AZV 398						SWP 10315, 22373
	AZV 456						
AZV 454	AZV 126	O V ^g	-0.19	-0.98	LWR 14948
							SWP 18909, 22016
AZV 488	AZV 398	B0 Ia ^f	-0.24	11.88	-0.13	-0.97	LWR 5642
	AZV 456						SWP 6590
AZV 504	AZV 20	B9 Ia ^f	...	11.91	-0.04	-0.46	LWP 19242
	AZV 211						SWP 40138
SK 194	AZV 20	B9 Ia ^f	...	11.74	+0.02	-0.53	LWP 21282, 83
	AZV 211						SWP 42507, 08

^a Brunet 1975.

^b Photometry from AZV82.

^c Crampton & Greasley 1982.

^d Humphreys 1983.

^e Garmany et al. 1987.

^f Ardeberg et al. 1972.

^g Prévot et al. 1984.

stars with the same optical spectral type but different metallicities may have different UV spectra. In addition, by using unreddened SMC objects, the foreground Galactic extinction is canceled if it is homogeneous across the SMC angular field. Subsequently, we have examined the UV lines to detect possible mismatches.

AZV 20 and AZV 211 have the same spectral type (A0 Ia), so we have used the same comparison stars, observed by us, for both of them (see Tables 4 and 5). Stars of spectral type A0 Ia present some difficulties. The UV spectra change rapidly with spectral type so that a mismatch has a much greater effect than it does for stars of earlier type. Furthermore, since stars of this spectral type are cooler and their UV flux lower, it is more difficult to get a good signal-to-noise ratio. AZV 126 has a spectral type (B0 Iw) very similar to that of AZV 398 (B2) and AZV 456 (B0-1), so there is an overlap in the comparison stars, taken from the *IUE* data archive, for all three (see Table 5). AZV 126, however, is the least reddened of these three stars; the comparison stars were selected in order to provide the largest possible difference between program and comparison stars (see next paragraph). The final list of comparison stars for each program star is as follows: for AZV 20 and 211, the comparison stars were AZV 161, 270, 504, and SK 194; for AZV 126, the comparison stars were AZV 61, 317, and 454; for AZV 398 and AZV 456, the comparison stars were AZV 235, 242, 289, 317, and 488.

As noted above, the *IUE* spectra have 1 Å sampling. The extinction calculated with such a small-wavelength step usually has a very poor signal-to-noise ratio. So we have also formed combined spectra with bins of 80 Å. The flux value in each 80 Å bin is assumed to be the sum of the fluxes in the 1 Å bins. The extinction curves are shown in Figures 2 and 3. The curves with 1 Å bins (Fig. 2) are useful for

identifying spectral type mismatches and the noisier regions. The curves in the figures are the weighted average of the curves using different comparison stars, and the error bars in the 80 Å curves (Fig. 3) are the average standard deviation. The weights used were the values of $\Delta(B-V)$, the difference between the program star and the comparison star colors given in Tables 4 and 5. In this way, we give greater weight to the reductions with the least reddened comparison stars. Also, this way of weighting is appropriate for errors dominated by measurement inaccuracies.

For AZV 211, we initially determined extinction curves from the four comparison stars listed above. We found, however, that the curve using the comparison star AZV 161 was very different than the other three curves, and we suspect that this comparison star may be reddened. Therefore, we have excluded the curve using AZV 161 from the average curve for AZV 211 and for AZV 20. The resultant average curve for AZV 211 seems to follow the SMC standard with no bump and an enhanced FUV extinction (Figs. 2c and 3c).

AZV 20 has the noisiest extinction curve (see Fig. 2a) in the sample, despite the fact that it has a large color excess (see Table 4). The systematic increase in error with increasing frequency is due to the systematic decrease in the signal-to-noise ratio (see Fig. 2a). Where the extinction curve is less noisy, the values of the extinction are close to those for the typical SMC extinction curve (compare, for example, Fig. 2a with Fig. 2c and Fig. 2d at $\lambda^{-1} \approx 5.5 \mu\text{m}^{-1}$). Its binned extinction curve shows bin-to-bin fluctuations larger than expected from the error bars.

The extinction curves that we have redetermined for AZV 398 (Figs. 2d and 3d) and AZV 456 (Figs. 2e and 3e) are in perfect agreement with those of Prévot et al. (1984) and Lequeux et al. (1984), respectively.

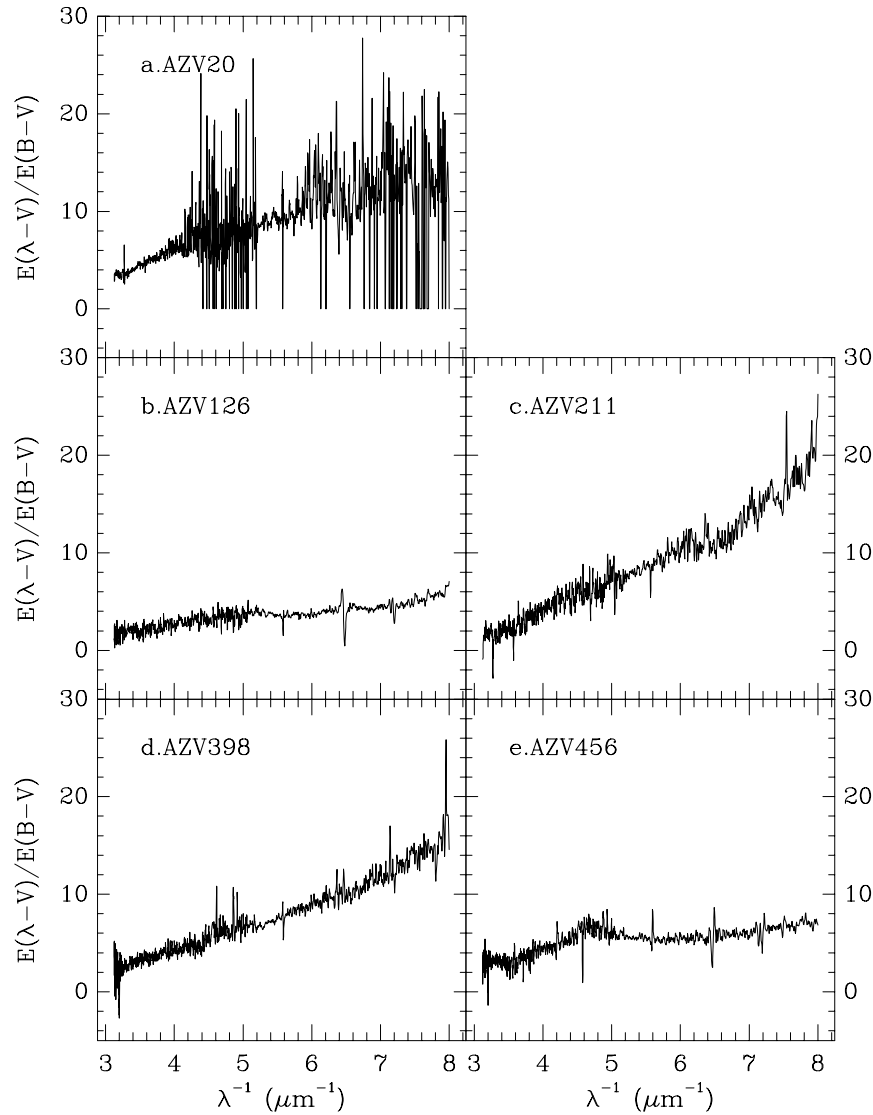


FIG. 2.—Extinction curves of SMC stars obtained using the pair method and combined spectra with 1 \AA sampling (except for 5 \AA sampling for AZV 126). The curves for AZV 398 and AZV 456 were derived in part using *IUE* images of these objects obtained by Prévot et al. (1984) and Lequeux et al. (1984).

The extinction for AZV 126 (Fig. 2b) will be discussed in § 4.1. AZV 215, for which we have obtained polarization data (Tables 1 and 3), has spectra available in the *IUE* data bank. However, it has a very small $(B-V)$ value, comparable to possible comparison stars, so we could not determine a reliable extinction curve for it.

3. QUALITATIVE STUDY OF OPTICAL POLARIZATION

3.1. Fits of Serkowski Law to SMC Polarization Data

Serkowski (1973; see also Coyne et al. 1974) has shown that the Galactic interstellar polarization can be described by the following expression:

$$P(\lambda) = P_{\max} \exp \left[-K \ln^2 \left(\frac{\lambda_{\max}}{\lambda} \right) \right], \quad (2)$$

where, from the observed data, the parameters P_{\max} , K , and λ_{\max} may be obtained.

P_{\max} , the maximum polarization, depends on the column density of dust, as well as the magnetic field structure and alignment efficiency along the line of sight; λ_{\max} is the wavelength where P_{\max} occurs, and it is related to the size of the

dust particles (Coyne et al. 1974; Chini & Krügel 1983). K describes the width of the polarization curve.

In his original work, Serkowski has taken K as a constant with a value of 1.15. Codina-Landaberry & Magalhães (1976) have shown that K varied for different lines of sight. Furthermore, from model fits they showed that K could be interpreted as being related to changes in the grain size along the line of sight. Wilking et al. (1980) and Wilking, Lebofsky, & Rieke (1982), using an extended wavelength range that included the IR, suggested a linear relation between K and λ_{\max} . Whittet et al. (1992), with an even larger sample, have provided the following relation:

$$K = (1.66 \pm 0.09)\lambda_{\max} + (0.01 \pm 0.05). \quad (3)$$

We have performed fits of the Serkowski relation to our SMC data in two ways: (1) allowing K to be a free parameter, and (2) using the above relation between K and λ_{\max} . Admittedly, the first approach results in larger uncertainties for the derived parameters, especially K , but we felt that a first comparison between the K values from the SMC data and those from Galactic data would be of interest. Furthermore, a comparison between the two methods might help to

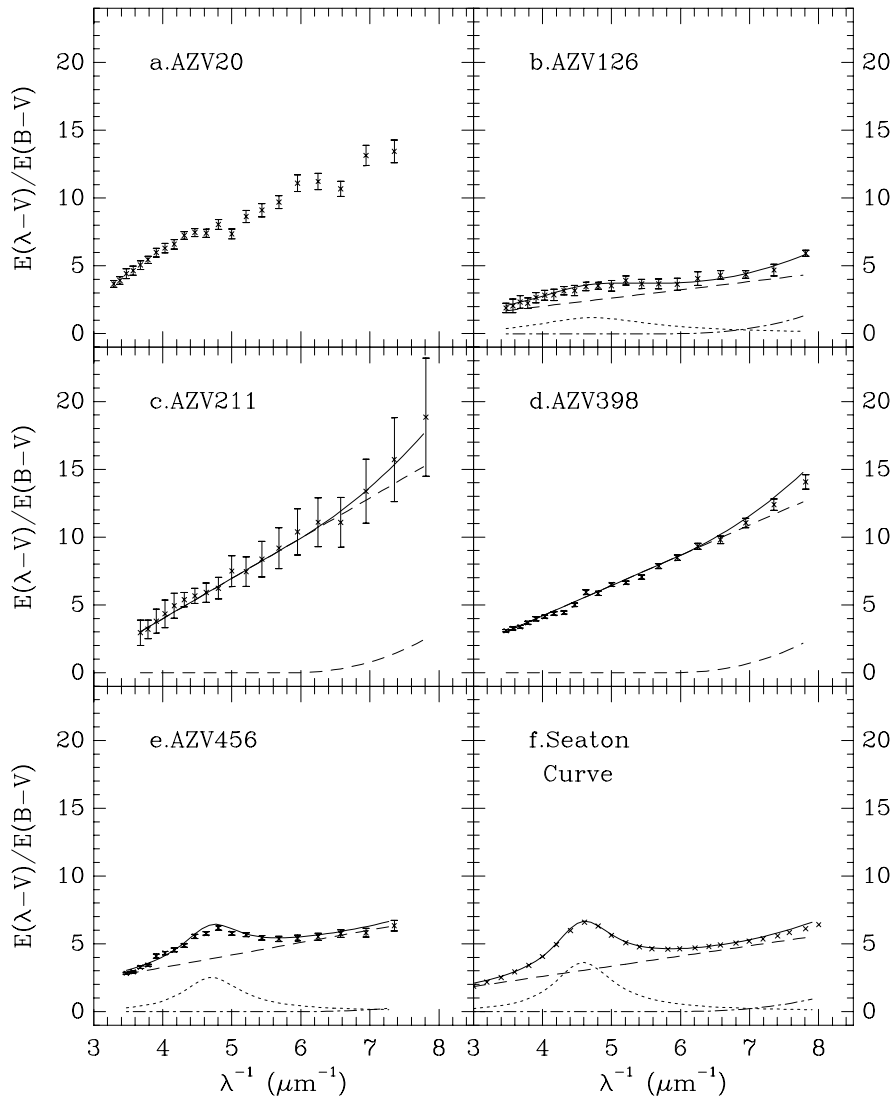


FIG. 3.—Parametric fits, using the Fitzpatrick & Massa (1986) representation, to the extinction curves for AZV 20, 126, 211, 398, and 456 and the Seaton curve for the Galaxy. The fits (*solid line*) were made to the extinction curve with a sampling of 1 \AA (except for 5 \AA sampling for AZV 126). The points with error bars represent the extinction curve with a binning of 80 \AA . The respective component curves are the linear portion (*dashed*), the Drude function (*dotted*), and the polynomial function for the UV and FUV (*dash-dotted*) (see eq. [5]).

judge the reliability of the derived parameters.

Table 3 gives the Serkowski fit parameters. In that table, the last three columns show, respectively, the reduced χ^2 , the associated probabilities, and the degrees of freedom. The actual fits are shown in Figure 1. The SMC polarization data can be well fitted by the Serkowski relation by using either the two- or the three-parameter method. The only fit significantly improved with three free parameters is that of AZV 456.

The values of λ_{\max} from the two methods agree well within the errors. P_{\max} from both fits shows an even closer agreement. Larger differences are found for the K parameter, although they still may be consistent within the large uncertainties. AZV 215 has data points at only four wavelengths, and hence the uncertainties in K are particularly large.

Table 3 shows that most of the SMC stars show λ_{\max} smaller than the Galactic average, $0.55 \mu\text{m}$. In particular, this is true for two of the stars with the best polarimetric

signal-to-noise ratio, AZV 211 and AZV 398, which also have a typical SMC extinction curve (§ 2.2.2). These results are in sharp contrast, for instance, with those for the LMC (Clayton & Martin 1985). For their sample of stars with measured extinction, the smallest observed λ_{\max} value is $0.52 \mu\text{m}$, with a median value of $0.58 \mu\text{m}$. Our results will be discussed further in § 6.

AZV 456, which has a UV bump (§ 4.1), and, to a certain degree, AZV 215 show λ_{\max} values close to the Galactic norm. The three-parameter fits (Table 3 and Fig. 1) indicate that their polarization curves are narrower than those for the other stars. The fact that the Serkowski fit to the “normal λ_{\max} ” polarization curve of AZV 456 is significantly poorer when we use the Galactic relation between K and λ_{\max} may suggest that there is a different relationship between these parameters in the SMC. This suggestion is somewhat strengthened by a plot of the K versus λ_{\max} taken from the three-parameter fits in Table 3 and shown in Figure 4. While the K - λ_{\max} relation for the SMC is similar

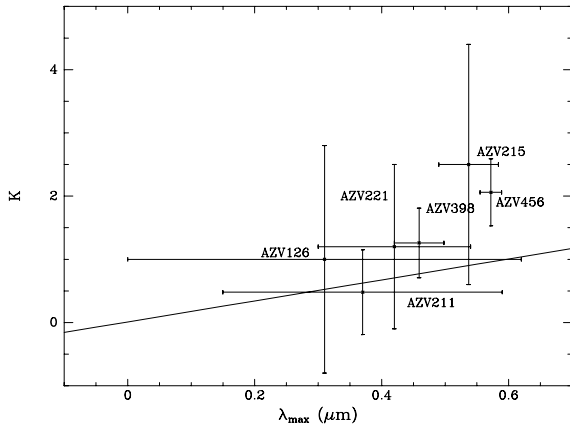


FIG. 4.— K vs. λ_{\max} for SMC stars (this work) from the three-parameter fits. The solid line is the Galactic relationship (Whittet et al. 1992).

to the Galactic one, a steeper slope is suggested. More data beyond the optical domain, and for more stars, are needed to clarify this.

3.2. Polarization and Visible Extinction

The maximum polarization toward a given line of sight is related to the available amount of dust and depends on factors such as the magnetic field direction, the grain alignment efficiency, and the polarizing efficiency of the grains. Empirically, it is verified that for the Galaxy (Serkowski, Mathewson, & Ford 1975),

$$P_{\max} \leq 9.0E(B-V). \quad (4)$$

A plot of P_{\max} versus $E(B-V)$ for our sample is given in Figure 5. We have used the two-parameter fit, P_{\max} values from Table 3. We have obtained the total color excesses (Table 4, col. [7]) using the spectral type-color relation by Brunet (1975). When both our estimates and other observed values were available (AZV 398 and 456; Bouchet et al. 1985), we used the latter. For AZV 215, we used the value of 0.12 mag (Bouchet et al. 1985). We have then corrected all color excesses by 0.05 mag to take into account the Galactic foreground reddening (§ 2.1.2; Bessel 1991). The above empirical relation between P_{\max} and the color excess for the Galaxy is the solid line plotted in Figure 5. It is seen that the SMC stars also obey the Galactic relation between P_{\max} and $E(B-V)$.

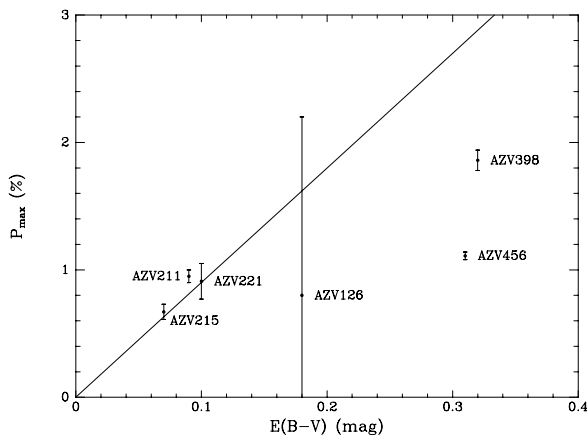


FIG. 5.—Polarization vs. $E(B-V)$. The continuous line represents the Galactic upper limit (see text, § 3.2, for discussion).

A related quantity of interest is the average ratio $P_{\max}/E(B-V)$ for the SMC objects. This is $7.2\% \text{ mag}^{-1}$ (from Tables 3 and 4). This value is comparable to the corresponding values for the Galaxy ($5.0\% \text{ mag}^{-1}$; Serkowski et al. 1975) and the LMC ($6.0\% \text{ mag}^{-1}$; Clayton & Martin 1985). Our average is biased because of our selection of the more highly polarized stars for this multi-wavelength study. In the near future, data from our survey in progress should be able to improve the estimate of this ratio for the SMC.

Serkowski et al. (1975) found a relationship between λ_{\max} and $R [=A(V)/E(B-V)]$, $R = 5.5 \lambda_{\max}$, for stars along several lines of sight in the Galaxy. Whittet & van Breda (1978), with the aid of infrared photometry, confirmed that relation and obtained $R = (5.6 \pm 0.3)\lambda_{\max}$. This correlation was reexamined and again confirmed by Clayton & Mathis (1988) using sight lines that included dense clouds as well as the more diffuse ISM. Using the data for AZV 211, 221 and 398, we obtain $\langle \lambda_{\max} \rangle = 0.40 \pm 0.02 \mu\text{m}$. From visual and near-IR photometry for stars in the SMC, Bouchet et al. (1985) obtained a value of $R = 2.72 \pm 0.21$, from which we obtain $R/\lambda_{\max} = 6.8 \pm 0.6$, still consistent with the Galactic relation. In other words, the somewhat smaller value of R for the SMC does translate into smaller values of λ_{\max} . Clearly more SMC data are needed to examine this relation further.

For AZV 456, the λ_{\max} values from the two- and three-parameter fits (Table 3, col. [2]), using the above Galactic relation between R and λ_{\max} , give 3.30 ± 0.24 and 3.19 ± 0.20 for R . In other words, the star with a ‘‘Galactic’’ extinction curve does suggest a larger value of R than that inferred from the typical SMC extinction. However, we have already pointed out in § 3.1 that AZV 456 does not seem to conform to the Galactic K versus λ_{\max} . In addition, we shall see in § 4.1 that neither does its extinction curve conform in detail to that expected from a larger value of R .

4. PARAMETRIC STUDY OF UV EXTINCTION

4.1. Parameterization

In order to analyze objectively the extinction curves for the SMC, we have fitted them for the first time by using the parameterization of Fitzpatrick & Massa (1986). However, we have fitted the parameters simultaneously, contrary to the approach of Fitzpatrick & Massa (1990). We have done this by minimizing the χ^2 . The parameterization of Fitzpatrick & Massa (1990) is expressed by

$$\frac{E(x-V)}{E(B-V)} = c_1 + c_2 x + c_3 D(x; \gamma, x_0) + c_4 F(x), \quad (5)$$

where

$$x = \lambda^{-1},$$

$$D(x; \gamma, x_0) = \frac{x^2}{(x^2 - x_0^2)^2 + x^2 \gamma^2},$$

and

$$F(x) = \begin{cases} 0.5392(x - 5.9)^2 + 0.05644(x - 5.9)^3 & \text{if } x \geq 5.9 \mu\text{m}^{-1}; \\ 0 & \text{if } x < 5.9 \mu\text{m}^{-1}. \end{cases}$$

We have not considered the star AZV 20 because of its very small signal-to-noise ratio extinction curve (see Fig. 2a

and discussion in § 2.2.2). We have performed the fits using the extinction curves with bins of both 1 Å (5 Å in the case of AZV 126) and 80 Å in order to check the dependency of the parameters on the bin size. The results are presented in Table 6 and in Figure 3, together with the results from the fit of the Galactic curve (Seaton 1979).

We now discuss the fits for each star with reference to Table 6 and according to the three parts of equation (5): the linear part, the Drude function fit to the bump $D(x; \gamma, x_0)$, and the exponential fit to the increasing extinction into the FUV. Column (14) of Table 6 gives the integral of the extinction curve over the bump.

AZV 211 and AZV 398 both show the typical SMC extinction (Prévot et al. 1984) with no bump and a rapid increase in the UV and FUV extinction (Table 6, col. [8]). Although these stars do not present the bump, any oscillation in the extinction curve might be interpreted artificially by the code as a small bump (see Table 6, cols. [10]–[13], and Fig. 3). For that reason, we also have performed the fits without the Drude function component. There was, however, no significant difference in the resultant parameters.

The extinction curve of AZV 456 is very similar to that for the Galaxy (Fig. 3; Lequeux et al. 1984; see entries for AZV 456 and the Galaxy in Table 6), and in fact its extinction curve has been often referred to as a “Galactic-type” curve. However, our fits show that its bump is shifted to the blue ($x_0 = 4.66 \pm 0.02 \mu\text{m}^{-1}$; Table 6) with respect to the Galactic average ($x_0 = 4.596 \pm 0.019 \mu\text{m}^{-1}$). For comparison, the largest value of x_0 in the sample of Fitzpatrick & Massa (1986) is $4.63 \mu\text{m}^{-1}$. The width and intensity of the bump for AZV 456 are within the range of those for the Galaxy. In contrast, the three sight lines that show $x_0 > 4.65 \mu\text{m}^{-1}$, seen through dense material, all appear to be associated with broad bumps (Cardelli & Savage 1988; Cardelli & Clayton 1991; Mathis 1994).

From studies of several Galactic sight lines, which included diffuse, dark cloud and star formation regions, Cardelli, Clayton, & Mathis (1989) have shown that there is an average extinction law over the wavelength range 3.5–0.125 μm that is applicable to such environments. This mean extinction law, $A(\lambda)/A(V)$, depends only on the parameter R . They have noted, however, that a few sight lines, which included ones with broad bumps and those toward the LMC, did not conform to such a law. In Figure 6, we plot the UV extinction curve of AZV 456 with the

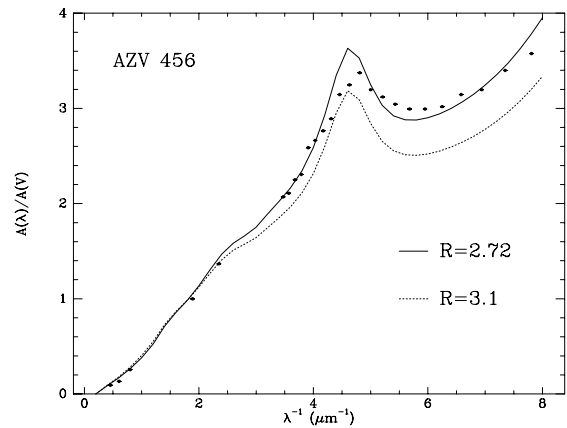


FIG. 6.—The extinction curve of AZV 456 with the analytical curves of Cardelli et al. (1989) for $R = 2.72$ (solid line) and $R = 3.1$ (dotted line) superimposed.

analytical law of Cardelli et al. (1989) for the values of $R = 2.72, 3.1$. It can be seen that the observed and analytical curves are discrepant, especially around the bump region, meaning that the line of sight to AZV 456 does not conform to the single parameter interpolation that performs well for the Galactic environs.

Among stars in our Galaxy that also present non-standard UV bumps, HD 62542 has the most extreme bump, centered at $4.74 \mu\text{m}^{-1}$ (Cardelli & Savage 1988). Interestingly enough, the FUV extinction curve of HD 62542 and the SMC are actually very similar. However, its bump is extremely shallow, and its intensity is quite different (lower) compared with the Galactic average and AZV 456. In addition, our multicolor polarimetry of HD 62542 (reported by Clayton et al. 1992) shows that its λ_{max} value is $0.59 \mu\text{m}$, quite different from the low λ_{max} values for the SMC (Table 3). This stresses the value of linear polarimetry in providing additional, independent information about the grains. In fact, in § 5 it will become clear that detailed, simultaneous fitting of both extinction and polarization is more restrictive on the grain model parameters.

The parameterization of the extinction curve for AZV 126 with 1 Å bins did not converge. This may have been due to the available signal-to-noise ratio or some spurious effect in the extinction curve that the parameterization fit tried to include. Hence, we have fitted equation (5) to an extinction curve binned to 5 Å for AZV 126. This allowed a more

TABLE 6
PARAMETERS OF THE SMC EXTINCTION CURVES USING EXPRESSION OF FITZPATRICK & MASSA 1990

Star (1)	c_1 (2)	σ_{c_1} (3)	c_2 (4)	σ_{c_2} (5)	c_3 (6)	σ_{c_3} (7)	c_4 (8)	σ_{c_4} (9)	γ (μm^{-1}) (10)	σ_γ (μm^{-1}) (11)	x_0 (μm^{-1}) (12)	σ_{x_0} (μm^{-1}) (13)	A (μm^{-1}) (14)	χ^2 (15)	Bin (Å) (16)
AZV 126	-2.2	7.3	0.68	0.44	47	282	0.71	0.58	4.4	7.7	4.70	0.68	16.80	0.17	80
	-0.42	0.18	0.61	0.03	4.97	2.00	0.49	0.06	2.05	0.31	4.72	0.05	3.81	1.40	5
AZV 211	-8.6	2.8	3.09	0.52	0.17	0.95	1.1	1.6	0.5	1.3	4.24	0.27	...	0.06	80
	-8.53	0.20	3.03	0.04	0.46	0.20	1.24	0.18	0.79	0.15	4.16	0.03	...	0.75	1
	-7.70	1.70	2.96	0.37	1.10	1.60	0.11	80
	-7.90	0.13	2.97	0.03	1.08	0.17	0.80	1
AZV 398	-4.67	0.23	2.21	0.05	-0.01	0.03	1.00	0.27	0.13	0.35	4.26	0.08	...	1.03	80
	-4.63	0.02	2.18	0.01	0.01	0.01	1.05	0.02	0.095	0.09	4.60	0.01	...	5.80	1
	-4.57	0.16	2.22	0.04	1.00	0.02	2.54	80
	-4.73	0.02	2.23	0.01	0.95	0.02	7.80	1
AZV 456	-0.57	0.20	0.90	0.04	4.7	1.0	0.17	0.13	1.34	0.13	4.66	0.02	5.51	1.57	80
	-0.44	0.02	0.92	0.01	2.70	0.06	0.09	0.01	1.04	0.01	4.71	0.01	4.10	9.70	1
Seaton curve	-0.4	2.0	0.75	0.31	4.0	4.4	0.22	0.54	1.05	0.55	4.59	0.12	5.98	0.02	...

reasonable parameterization. It nevertheless shows an abnormally small slope for the linear part (Table 6, col. [4]). The Drude function fits (Table 6, cols. [10]–[13]) indicate that it may have the extinction bump, but it may be shifted to the blue (Table 6, col. [12]) with regards to both the Galaxy and AZV 456. The bump is also abnormally wide (Table 6, col. [10]), although its intensity is within the Galactic range. The rise into the UV and FUV (Table 6, col. [8]) is intermediate between that typical for the SMC and that for the Galaxy. The extinction curve for AZV 126 has a large intrinsic uncertainty, and it must be viewed with caution.

4.2. Correlations between Extinction Components

Although the small number of extinction curves available for the SMC makes any search for correlations between the parameters difficult, there are tentative indications of correlations between the linear coefficients (c_1 , c_2) and the coefficient (c_4) of the linear and FUV portions, respectively, of the extinction curves (eq. [5]). These are shown in Figure 7. The point with large error bars in that figure corresponds to parameters for the Galactic curve given in Table 6. The large errors are due to the fact that relatively few data points were tabulated conveniently for the fit to the Galactic curve. Hence, those error bars are very conservative.

Figure 7 shows that the FUV curvature for the SMC, c_4 , is anticorrelated with the constant component, c_1 , and positively correlated with the slope of the linear component, c_2 .

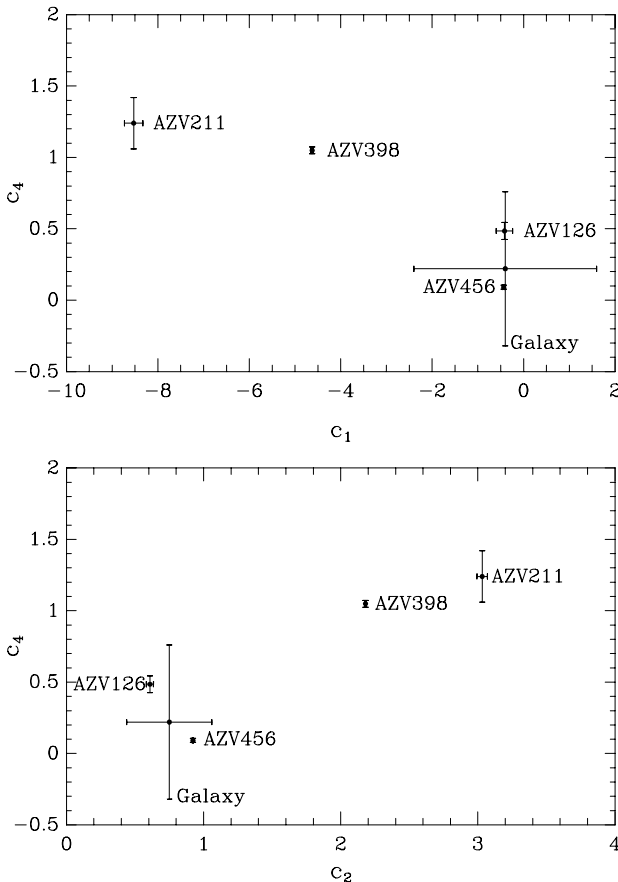


FIG. 7.—The coefficient, c_4 , for the exponential UV and FUV parts of the extinction curve plotted against the coefficients, c_1 and c_2 , respectively, for the linear part of the extinction curve (see eq. [5]).

In fact, the parameters c_1 and c_2 are correlated perfectly (Fitzpatrick & Massa 1988; Jenniskens & Greenberg 1993), and c_1 is not an independent parameter. If the FUV curvature does increase at the same time as the contribution of the linear component to the extinction, this can be interpreted as the result of a simultaneous decrease in the average size of the grains responsible for these various parts of the extinction curve. For the Galaxy, no correlation is found between the linear rise and the extinction in the FUV (Jenniskens & Greenberg 1993). This may be a further indication of the differences between the ISM in the SMC and the ISM in the Galaxy, where the correlation found may simply signify the increasingly larger number of smaller particles as we go from the Galaxy to the SMC.

The fact that AZV 211 and AZV 398 show a sizable contribution to the FUV term in their extinction curves, quite larger than that of AZV 456, is consistent with what is found for the Galaxy, for which no positive correlation exists between the bump and the FUV curvature (Greenberg & Chlewicki 1983; Jenniskens & Greenberg 1993). In the Galaxy, the linear rise part (c_1 , c_2) of the extinction curve is systematically less in dense media (Cardelli et al. 1989; Jenniskens & Greenberg 1993). The behavior of the extinction curve for AZV 456 seems to follow the same trend. In contrast, the Galactic object HD 204827 shows a steep FUV rise (Fitzpatrick & Massa 1990) while at the same time showing small λ_{\max} (Whittet et al. 1992; Clayton et al. 1995), in line with the typical SMC sight lines. In § 6, we will return to this discussion.

5. SMC DATA AND DUST MODELS

We have tried to fit the SMC data using the MRN grain model. In this model, the grains are homogeneous, spherical particles of silicate and of graphite with a -3.5 power-law size distribution. The sizes range from 0.02 to 0.25 μm for silicate grains and from 0.005 to 0.25 μm for graphite grains. There are two approaches to the polarization within the context of the MRN model. Mathis (1979, 1986) introduced an additional population of elongated silicate grains (cylinders). A single size distribution describes both the spherical and the elongated silicates. From a minimum grain radius, a_{-}^{sil} , until an intermediate radius, a_{p}^{sil} , the grains were assumed to be spherical (or not aligned), and from then up to a maximum radius, a_{+}^{sil} , they were taken as aligned cylinders. This case will be called the M79 model. Mathis (1986, the M86 model) proposed a modification to the above scenario. The polarizing material would consist of silicate particles containing inclusions of ferromagnetic material in order to make the alignment more efficient (Jones & Spitzer 1967). The number of these inclusions increases with grain size in such a way that larger grains have a greater probability of being aligned. Although the size distribution is the same as in the M79 model, in this case there is a probability function that must be multiplied by the size distribution of cylinders in order to give the number of aligned cylindrical grains contributing to the polarization. To calculate the extinction in the M86 model, we have assumed that all cylindrical grains are aligned.

We introduce two innovations to the above models. First, we attempt to fit the observations by using the polarization and the extinction together. The implications on the extinction curve of including silicate cylinders has not been studied in detail by Mathis (1979, 1986). Kim & Martin (1994, 1995) have derived the dust particle mass distribution

from the polarization curve for the Galaxy, although, as noted by them, extinction and polarization curves still need to be interpreted consistently and simultaneously. Thus, to the best of our knowledge, such combined fits have not been attempted previously. To carry out these fits, it is necessary for us to adopt a model for the degree of alignment as a function of grain size, and an axial ratio for the aligned grains. At the end of the fitting process, we look at the predicted ratio $P(V)/A(V)$ to check the validity of these assumptions. It is important to realize (§ 5.2) that the combination of shapes may affect the extinction in addition to the polarization. Second, we introduce *volume* continuity as an alternative to *size* continuity. The size distribution, $n(a)$, can be represented algebraically as $n(a) = Nf(a)$, where a is the particle radius and $f(a)$ describes the shape of the size distribution. N , hereafter called the number constant, is related to the absolute number of grains. This constant is dependent on the elemental abundance (gas phase plus dust) and on the depletion of the main grain constituents. We use the word depletion to mean the fraction of a given chemical element locked up in the grains. The abundances of interest are those of carbon (C) and silicon (Si).

In the single size distribution of Mathis (1979), when silicate cylinders and spheres have the same number constant, the Si fraction in each population is fixed automatically by one boundary condition: the number of cylinders and spheres at the radius a_p^{sil} must be the same. Hereafter, we call this case *size continuity*. In addition, we have studied the influence of a different boundary condition on the distribution of spheres and cylinders. We employ the same shape, $f(a)$, for the size distributions of both populations, but their number constants are different. Specifically, we have calculated them in such a way that the volume distribution is continuous, i.e., the boundary condition is such that the total volume occupied by the spherical and by the cylindrical grains of size a_p^{sil} must be equal. This will be called *volume continuity*. For example, for the elongation of the two adopted here for the cylindrical particles, the number of spheres is larger by a factor 3. This results in a larger relative contribution by spherical particles in the case of the volume continuity as compared with size continuity.

The optical properties for the so-called astronomical silicate have been taken from Draine & Lee (1984), who made a synthesis of laboratory and astronomical data. Its properties are quite similar to olivine ($[\text{Mg}, \text{Fe}]_2\text{SiO}_4$), and it shows the characteristic change in the UV slope of the extinction curve around $6.5 \mu\text{m}^{-1}$. For enstatite ($[\text{Mg}, \text{Fe}]\text{SiO}_3$), we have used the optical constants obtained by Huffman & Stapp (1971). These constants are given only for the optical and UV. This material was employed by Bromage & Nandy (1983) in their fit to the typical extinction curve for the SMC. The index of refraction for graphite has been taken from Draine & Lee (1984). We use the “ $\frac{1}{3}-\frac{2}{3}$ ” approximation to calculate the extinction coefficients. Draine & Malhotra (1993) have shown recently that this procedure is sufficiently accurate. For the amorphous carbon, we have adopted the constants of Duley (1984).

5.1. Fit Procedure

Our approach was to first fit the polarization, the wavelength dependence of which determines the size distribution parameters of the cylindrical silicate population. Then from the maximum polarization of the fit, we determine the Si abundance in the form of cylindrical grains. Next, we fitted

the size distribution parameters of graphite and spherical silicate grains in order to reproduce the extinction curve, assuming the cylindrical population is fixed.

The minimum and maximum sizes of the cylinder silicate distribution were obtained from a χ^2 minimization procedure applied to the polarization curve normalized to the maximum polarization. We assumed perfect spinning alignment (Chlewicki & Greenberg 1990 and references therein) and three values of the angle between the direction of the magnetic field and the plane of sky, γ : 10° , 30° , and 60° . Next, we calculated the necessary Si abundance (i.e., Si/H) to reproduce the polarization in the V filter. For that, we must know the color excess, $E(B-V)$, and the gas-to-dust ratio, $N(\text{H})/E(B-V)$ (e.g., Casey 1991), since we in effect are fitting $P(V)/N(\text{H})$. Assuming a given continuity (size or volume), we can calculate the number constant of the spherical silicate distribution, whose maximum size is fixed by the cylinder sizes. Therefore, for a given C depletion, we have only to fit the minimum size of spherical silicates and the size parameters of the C grain population (again, the slope of the size distribution was held fixed, for simplicity). We also apply a χ^2 minimization procedure to the $A(\lambda)/N(\text{H})$ data. All the extinction curves were fitted using both size and volume distribution continuities and various carbon depletions.

5.2. Fits to Galactic Data

In order to compare the SMC environment with that of the Galaxy, we first discuss fits to the polarization and extinction in the latter. In Figure 8 and Table 7, we present fits to the polarization curve that was considered as a Serkowski law with $\lambda_{\text{max}} = 0.55 \mu\text{m}$ from optical studies. Presently, the interstellar polarization curve is known throughout a much wider wavelength range, which could provide stronger constraints on the size distribution (e.g., Kim & Martin 1994; Anderson et al. 1997). However, we decided to consider only the optical range, which is the one we have available for the SMC (§ 2.1). Obtaining the value of $P(V)/N(\text{H})$ to fit, we adopted $P_{\text{max}}/E(B-V) = 9$ [the maximum observed, and $P(V) \approx P_{\text{max}}$], $N(\text{H})/E(B-V) = 5.848 \times 10^{21} \text{ cm}^{-2}$ (Bohlin, Savage, & Drake 1978), and $R = 3.1$. The fractional error in $P(\lambda)$ was taken to be 10%. In Figure 9, the scale of P is in fact arbitrary, corresponding to $N(\text{H}) = 6.433 \times 10^{20} \text{ cm}^{-2}$, or $E(B-V) = 0.11$. We have assumed the following abun-

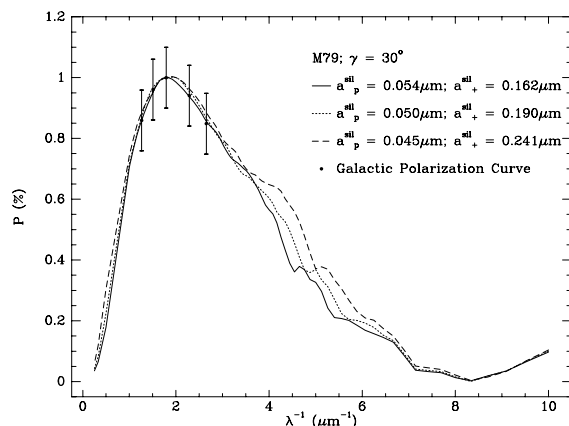


FIG. 8.—Fits to the Galactic polarization curve for $\gamma = 30^\circ$. The different curves are for size parameters representing local χ^2 minima (Table 7).

TABLE 7
PARAMETERS OBTAINED FROM FITS TO THE POLARIMETRIC DATA FOR THE SMC AND THE GALAXY

Object (Figure) (1)	a_p^{sil} (μm) (2)	a_s^{sil} (μm) (3)	$\langle a \rangle$ (μm) (4)	Width (μm) (5)	$\delta(\text{Si})^a$ (dex) (6)	Model (7)	Material (8)	γ (deg) (9)	χ^2 (10)	
Galactic polarization curve (Fig. 8).....	0.043	0.150	0.063	0.107	7.61	M79	AS	60	0.00003	
	0.039	0.186	0.059	0.147	7.66	M79	AS	60	0.00293	
	0.054 ^b	0.162	0.078	0.107	7.09	M79	AS	30	0.00035	
	0.050 ^b	0.190	0.074	0.140	7.13	M79	AS	30	0.00041	
	0.045 ^b	0.241	0.069	0.197	7.19	M79	AS	30	0.00267	
	0.062	0.203	0.090	0.141	6.98	M79	AS	10	0.00023	
	0.062	0.198	0.090	0.136	6.98	M79	AS	10	0.00027	
	0.086	0.143	0.106	0.057	6.93	M79	AS	10	0.00356	
	0.021	0.146	0.062	0.125	8.06	M86	AS	60	0.02490	
	0.015	0.146	0.057	0.131	8.10	M86	AS	60	0.02406	
	0.010	0.146	0.052	0.136	8.14	M86	AS	60	0.02394	
	0.006	0.146	0.048	0.140	8.17	M86	AS	60	0.02395	
	0.042	0.129	0.075	0.087	7.37	M86	AS	30	0.01162	
	0.026	0.146	0.066	0.120	7.44	M86	AS	30	0.01045	
	0.020	0.148	0.061	0.128	7.48	M86	AS	30	0.01037	
	0.010	0.148	0.052	0.138	7.54	M86	AS	30	0.01031	
	0.083	0.139	0.106	0.056	7.01	M86	AS	10	0.00312	
	0.061	0.163	0.095	0.101	7.08	M86	AS	10	0.00058	
	0.030	0.179	0.073	0.149	7.22	M86	AS	10	0.00076	
	AZV398 (Fig. 10)	0.031	0.149	0.048	0.119	6.46	M79	AS	60	1.62
0.037 ^b		0.172	0.057	0.135	5.96	M79	AS	30	1.57	
0.060		0.136	0.081	0.076	5.75	M79	AS	10	1.11	
0.043		0.088	0.056	0.046	6.56	M79	ENS	60	0.34	
0.045		0.186	0.069	0.141	6.21	M79	ENS	30	1.50	
0.061 ^b		0.099	0.075	0.038	6.07	M79	ENS	30	0.34	
0.076		0.141	0.098	0.065	5.99	M79	ENS	10	1.26	
0.031		0.082	0.047	0.051	6.64	M86	AS	60	0.48	
0.009		0.140	0.032	0.131	6.79	M86	AS	60	2.36	
0.031		0.168	0.053	0.137	6.10	M86	AS	30	1.63	
0.034		0.202	0.058	0.168	5.94	M86	AS	10	1.69	
0.031		0.162	0.054	0.131	6.89	M86	ENS	60	1.71	
0.042		0.089	0.057	0.047	6.77	M86	ENS	60	0.59	
0.042		0.195	0.066	0.153	6.31	M86	ENS	30	1.58	
0.062 ^b		0.098	0.075	0.036	6.14	M86	ENS	30	0.38	
0.078		0.136	0.098	0.058	5.99	M86	ENS	10	1.44	
AZV456 (Fig. 12)		0.045	0.145	0.066	0.108	7.10	M79	AS	60	6.43
		0.056	0.160	0.080	0.104	6.58	M79	AS	30	7.24
		0.099 ^b	0.131	0.112	0.032	6.40	M79	AS	10	1.93
		0.109 ^b	0.166	0.131	0.057	7.56	M79	ENS	60	2.21
	0.047	0.202	0.072	0.155	7.41	M79	ENS	60	10.07	
	0.131	0.173	0.149	0.042	6.99	M79	ENS	30	12.94	
	0.062	0.192	0.090	0.130	6.87	M79	ENS	30	10.29	
	0.084	0.200	0.116	0.116	6.71	M79	ENS	10	4.67	
	0.112 ^b	0.145	0.126	0.032	6.65	M79	ENS	10	1.72	
	0.038	0.144	0.075	0.107	7.51	M86	AS	60	11.44	
	0.047	0.157	0.084	0.111	6.87	M86	AS	30	10.72	
	0.055	0.184	0.094	0.129	6.65	M86	AS	10	6.52	

NOTE.—Col. (1): the object name in the AZV82 catalog. Col. (2): the minimum size of cylindrical grain. Col. (3): the maximum size of cylindrical grain. Col. (4): average size. Col. (5): width of the size distribution that corresponds to the difference between the two size parameters. Col. (6): silicon abundance needed to reproduce the degree of polarization. Col. (7): models: M79 (Mathis 1979) or M86 (Mathis 1986). Col. (8): material used in the calculations: AS (astronomical silicate) or ENS (enstatite) (see § 2 for references). Col. (9): angle between the magnetic field and the plane of sky. Col. (10): the value of χ^2 is not divided by N .

^a The observed values of the Si/H abundance for the Galaxy (Anders & Grevesse 1989) and the SMC (Dufton et al. 1990) are 7.55 and 6.88, respectively.

^b The fits in this row are plotted in the figures whose numbers are given in col. (1).

dances: $\text{Si}/\text{H} = 3.55 \times 10^{-5}$ (7.55 dex) and $\text{C}/\text{H} = 3.63 \times 10^{-4}$ (8.56 dex) (Anders & Grevesse 1989). In Figure 8, we show fits for $\gamma = 30^\circ$, although the wavelength dependence of the Galactic polarization curve is well fitted for all γ values used. We found local χ^2 minima for the various size distributions listed in Figure 8. Below we will study the behavior of the extinction curve for these different cylinder size distributions. The different size parameters obtained for a given γ differ in range but have practically the same $\langle a \rangle$ (Table 7). For $\gamma = 60^\circ$, the required Si abundance is greater than that available in the Galactic ISM. In this case, we

have assumed a $P_{\text{max}}/E(B-V)$ of 2.0 and 5.0 (Table 8, col. [16]). This lowers the amount of Si needed to fit the polarization.

We now proceed with fits to the Galactic extinction curve. These are shown in Figure 9 and Table 8. We see from Table 8 that the best fit to the Galactic extinction curve for each cylinder parameter set is found systematically for a carbon depletion of about 0.70 and volume continuity (Fig. 9). The curves depart from the observed Galactic curve in the optical range, and this is due to the adopted size distribution, as demonstrated by Kim, Martin,

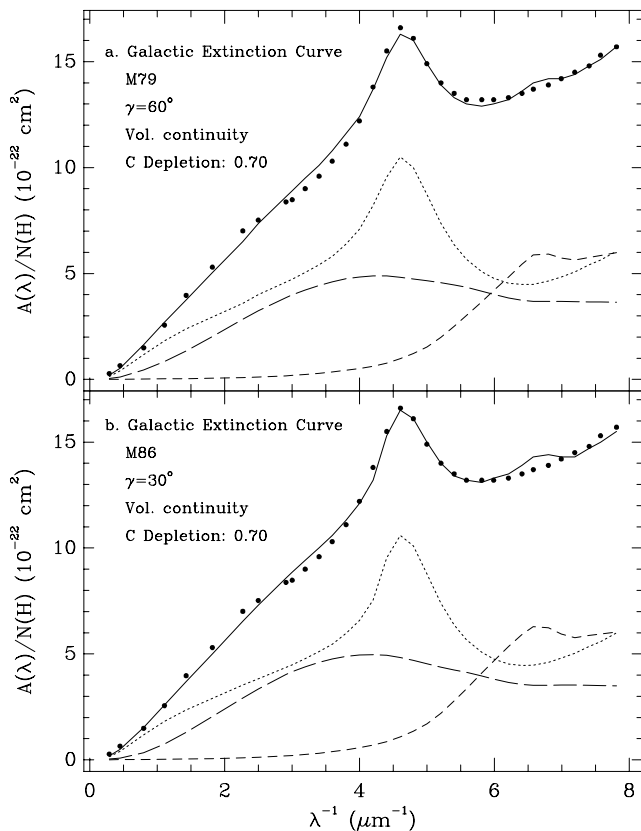


FIG. 9.—Best fits to the Galactic extinction curve (filled circles) using cylinder sizes derived from the (a) M79 or (b) M86 model fits. Additional fit parameters are given in Table 8. The dotted line represents the contribution of graphite; the long-dashed line represents the contribution of silicate cylinders; the short-dashed line represents the contribution of silicate spheres; and the solid line represents the total extinction.

& Hendry (1994). The better agreement of the extinction curve using volume continuity would seem to favor a situation in which the smaller grains are more numerous than predicted by the power law of index -3.5 . This may be accomplished by a steeper power law or a discontinuous size distribution from spheres to cylinders, as we assumed.

In any case, an important point is that, if we start with the size distribution of spherical silicates that, together with graphite, fit the extinction curve, a simple replacement of the larger silicate particles by cylinders that fit $P(\lambda)$ will *not* fit the extinction any longer.

A glance through the fits for the Galaxy in Table 8 reveals that there is a tendency of both the M79 and M86 models with perfect spinning alignment to provide relatively high $P(V)/A(V)$ values. This would indicate that perfect spinning alignment is not a necessity (see also Kim & Martin 1995).

5.3. SMC Fits

We have performed polarization and extinction fits for two stars in the SMC, AZV 398 and AZV 456, since they have relatively high values of polarization and better determined extinction curves. Furthermore, they may represent lines of sight with different grain characteristics. Although their UV extinction curves are different, their IR extinction seems to be very similar according to Bouchet et al. (1985). Hence, we have used the value of R ($=2.72$) from the latter reference. The abundances of carbon ($C/H = 6.455 \times 10^{-5}$, or 7.80 dex) and silicon ($Si/H = 7.59 \times 10^{-6}$, or 6.88 dex)

have been taken from Dufton, Fitzsimmons, & Howarth (1990), which provides the abundances of C, Si, and other elements in the atmosphere of a main-sequence, B-type star in the SMC. We assume that these represent the present ISM abundance in that galaxy (Pagel 1993). For our subsequent analysis, we assumed the following $N(H\ I)/A(V)$ values: for AZV 398, $4.1 \times 10^{22} \text{ cm}^{-2}$; for AZV 456, $6.9 \times 10^{21} \text{ cm}^{-2}$ (Bouchet et al. 1985).

5.3.1. AZV 398

In Figure 10 and Table 7, we present the model fits to the polarization of AZV 398 that show the highest polarization in our SMC sample (§ 2.1). The polarization decreases rapidly from the R to the I filter and not all of the models fit those points equally well. We also performed the fits by replacing astronomical silicate with enstatite. The value of $\langle a \rangle$ obtained with enstatite is slightly larger than that obtained using astronomical silicate as a consequence of the differences in optical constants of those materials.

In Figure 11 and Table 8, we present the model fits to the extinction of AZV 398. We obtain a good fit by using enstatite plus graphite and volume continuity (Table 8 and Fig. 11a). In this case, the extinction curves of each population can be combined to give a practically linear curve; 40% of the available C in the SMC is used. This fit, however, requires approximately 30% more Si than that available in the SMC ISM (Table 8, col. [14]). The relatively high value of the lower limit of the graphite size distribution ($0.0372 \mu\text{m}$, Table 8) of this fit, which prevents the extinction curve to show an UV bump, is also of note.

We have examined the consequences of replacing the population of graphite grains by one of amorphous carbon particles. As seen in Figure 11b, we can reproduce the AZV 398 extinction curve in shape and level. The amorphous carbon extinction fits the FUV especially well, and because of that, the fits with large C depletion tend to have smaller χ^2 . Also, we have obtained a larger number of good fits with amorphous carbon compared with fits using graphite. The required amount of Si and C in grains is about 70% and 80%, respectively, of that available in the SMC (Table 8).

The required mass in solid carbon obtained from the AZV 398 fits (note a in Table 8; Fig. 11) varies from 10% (with graphite) to 20% (with amorphous carbon) of the cor-

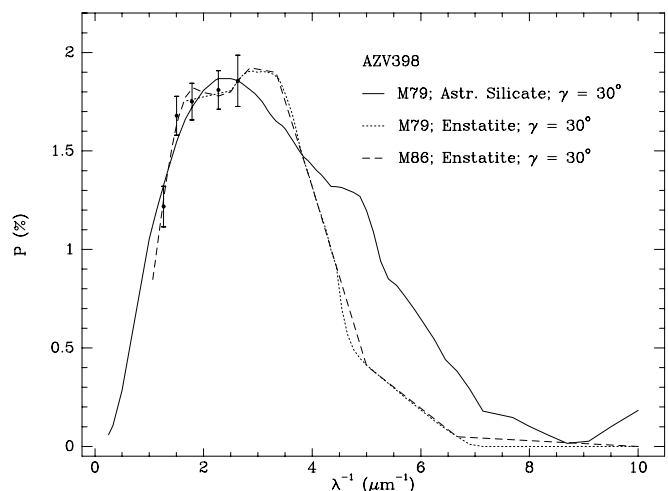


FIG. 10.—Fits to the AZV 398 polarization curve. The fit parameters are given in Table 7.

TABLE 8
PARAMETERS OBTAINED BY FITTING EXTINCTION CURVES

OBJECT (FIGURE) (1)	MODEL (2)	γ (deg) (3)	CONTINUITY (4)	CARBON DEPLETION (5)	SILICATE			CARBON			Si FRACTION			$P(V)/A(V)$	
					a^{sil} (μm) (6)	a_p^{sil} (μm) (7)	a^{sil} (μm) (8)	a^{car} (μm) (9)	a^{car} (μm) (10)	χ^2 (11)	Spherical Grains (12)	Cylindrical Grains (13)	Total (14)	Model (%/mag) (15)	Observed (%/mag) (16)
Galactic extinction curve (Fig. 9)	M79/AS + GR ^a	60	v	0.7	0.0174	0.043	0.150	0.0002	0.292	0.8	0.27	0.64	0.90	1.72	1.61
	M79/AS + GR	60	v	0.7	0.0124	0.039	0.186	0.0001	0.262	1.2	0.26	0.72	0.97	1.62	1.61
	M79/AS + GR	10	v	0.7	0.0151	0.086	0.143	0.0027	0.187	2.4	0.48	0.24	0.72	3.49	2.90
	M86/AS + GR	60	v	0.7	0.0046	0.021	0.146	0.0003	0.300	1.7	0.24	0.72	0.96	0.72	0.64
	M86/AS + GR ^a	30	v	0.7	0.0205	0.042	0.129	0.0001	0.301	0.9	0.27	0.66	0.93	3.17	2.90
	M86/AS + GR	30	v	0.7	0.0080	0.026	0.146	0.0001	0.306	2.4	0.25	0.78	1.03	3.12	2.90
	M86/AS + GR	10	v	0.8	0.0241	0.083	0.139	0.0068	0.259	1.3	0.45	0.29	0.74	3.09	2.90
	M86/AS + GR	10	v	0.8	0.0096	0.061	0.163	0.0035	0.170	3.1	0.33	0.34	0.67	3.04	2.90
	M79/AS + AC	60	v	1.0	0.0234	0.031	0.149	0.0148	0.021	57.0	0.04	0.38	0.42	2.05	2.01
	M79/AS + AC	30	s	1.0	0.0001	0.037	0.172	0.0123	0.041	157	0.03	0.12	0.15	2.56	2.01
AZV 398 (Fig. 11).....	M79/AS + AC	10	v	1.0	0.0119	0.060	0.136	0.0079	0.048	172	0.08	0.07	0.15	2.60	2.01
	M79/EN + GR ^a	60	v	0.4	0.0035	0.043	0.088	0.0372	0.140	29.4	0.79	0.48	1.27	1.89	2.01
	M79/EN + AC	60	v	0.8	0.0101	0.043	0.088	0.0036	0.531	50.8	0.57	0.48	1.05	1.84	2.01
	M79/EN + AC	30	v	1.0	0.0001	0.045	0.186	0.0040	0.050	113	0.20	0.21	0.41	2.48	2.01
	M79/EN + AC ^a	30	v	0.8	0.0001	0.061	0.099	0.0025	0.111	27.0	0.54	0.15	0.69	1.98	2.01
	M79/EN + AC	10	v	1.0	0.0001	0.076	0.141	0.0003	0.062	105	0.34	0.13	0.47	2.64	2.01
	M86/AS + AC	60	v	0.5	0.0001	0.009	0.140	0.0125	0.014	50.7	0.25	0.81	1.06	2.15	2.01
	M86/AS + AC	10	v	1.0	0.0056	0.034	0.202	0.0112	0.043	163	0.05	0.11	0.16	2.54	2.01
	M79/EN + GR ^a	60	s	0.15	0.0180	0.109	0.166	0.011	0.041	66.5 ^b	0.68	0.80	1.48	1.35	1.34

NOTE.—Col. (1): object. Col. (2): model for the polarizing grains (M79 or M86) and composition of the grains (AS stands for Astronomical Silicate, EN for ENstatite, GR for GRaphite, and AC for Amorphous Carbon). Col. (3): angle between the the magnetic field and the plane of sky. Col. (4): the continuity adopted (s = size continuity and v = volume continuity; see § 5). Col. (5): carbon depletion as a fraction of the available ISM abundance. Col. (6): minimum size of spherical silicate grains. Col. (7): maximum size of spherical silicate grains (= minimum size of cylindrical silicate grains). Col. (8): maximum size of cylindrical silicate grains. Col. (9): minimum size of carbon grains. Col. (10): maximum size of carbon grains. Col. (11): reduced χ^2 as a parameter of the fit quality. Si fraction abundances relative to the available in the SMC in form of spherical grains (col. [12]), cylindrical grains (col. [13]), and total fraction (col. [14]). Col. (15): $P(V)/A(V)$ obtained from the fit. Col. (16): observed $P(V)/A(V)$.

^a The entries in this row are plotted in the figures whose numbers are given in col. (1).

^b Assuming $N(H)/A(V) = 4.1 \times 10^{22} \text{ cm}^{-2}$ (see § 5.3.2).

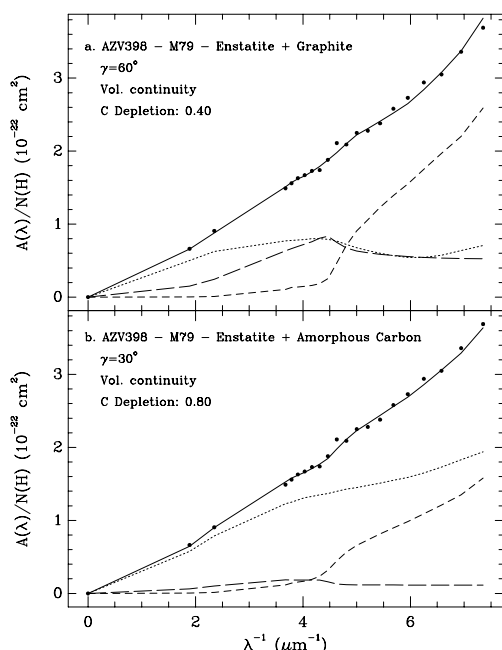


FIG. 11.—Best fits to the AZV 398 extinction curve using (a) graphite or (b) amorphous carbon. The fit parameters are given in Table 8. The line styles are the same as in Fig. 9.

responding value derived from the fits to the Galaxy. They reflect the product (C abundance) \times (required depletion) from the Galaxy to the SMC. Since the required depletions are similar from one galaxy to another, that value follows basically the C abundance ratio between the two galaxies. The same occurs with the total grain mass (carbonaceous + silicate grains). However, in the SMC, the fraction of mass in cylindrical grains relative to the total silicate grain mass (38% with graphite and 22% with amorphous carbon) is significantly smaller compared with the corresponding value in the Galaxy (about 70%). Also, the upper limit of the carbon particle size distribution (Table 8, col. [10]) is significantly smaller than that in the Galaxy for most of the (and certainly for the best) SMC fits. The amorphous carbon size distribution is also narrower than that for the Galaxy. In other words, the dust particles are on average smaller in the SMC as compared with the Galaxy. At the same time, note the absence of the very small graphite particles that produce an extinction bump.

Another important corollary of these AZV 398 fits is that the typical SMC extinction curve cannot be fitted adequately by using silicates alone, as previously advocated (Bromage & Nandy 1983; Pei 1992), unless the Si abundance in the SMC ISM is revised significantly upward, an unlikely event. Therefore, we feel that use of the dust properties of models that employ silicates only should be exercised with caution.

5.3.2. AZV 456

In Figure 12 and in Table 7, we present some of the best fits obtained for AZV 456, which has an unusually narrow polarization curve. These occur for either small values of γ or relatively narrow size distributions. The M79 fit with $\gamma = 10^\circ$ and astronomical silicates (*solid line*) presents a significant improvement relative to the $\gamma = 60^\circ$ fit with enstatite (*dotted line*). At the same time, the low- γ fits require less Si and provide less extinction (see below). Values of γ

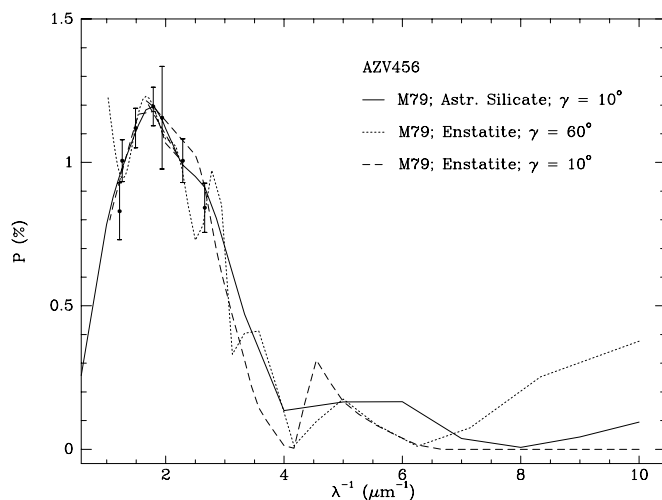


FIG. 12.—Fits to the AZV 456 polarization curve. The fit parameters are given in Table 7.

smaller than 10° were also tried but did not improve the fits. Some curves from models with narrow size distributions present an oscillating spectral dependence, especially for larger values of γ . The polarization curve of a single grain is characterized by ripples that usually are averaged out by a size distribution, except when the distribution is very narrow.

These fits are characterized by average sizes similar to those for the Galaxy, confirming the usual relationship between λ_{\max} and the average sizes. Wilking et al. (1980) suggested that an increase in the real part of the index of refraction can produce progressively narrower polarization curves. We have made some fits using hypothetical compounds, with a wavelength-independent index of refraction, in order to gain some insight into this. We have varied the real part of the index of refraction from 1.7 to 2.0 and the imaginary part from 0.01 to 0.05, but such changes in the index of refraction do not seem to be large enough to improve the results. Spheroids provide narrower polarization curves than do infinite cylinders (Wolff et al. 1994; Kim & Martin 1995). It remains to be verified whether these particle types can improve the fits.

Fitting the extinction of AZV 456 presents an interesting challenge, given a Galactic gas-to-dust ratio and the low SMC metallicity. We first try, as usual, to fit AZV 456 with silicate cylinders and spheres and with carbon spheres, but because of the observed UV bump, we must now add graphite spheres. The cylinders already use a sizable fraction of the available Si (Table 7, col. [6]). Providing the observed extinction levels by adding spherical particles will require the addition of Si several times that available in the SMC. Graphite particles reproduce the bump and provide some optical extinction, with a relatively small UV contribution. It is clear that there will not be enough material available in the SMC ISM capable of providing the needed extinction toward AZV 456.

A possible solution out of this conundrum is to resort to the possibility that AZV 456 actually may have a larger gas-to-dust ratio, closer to the more typical SMC values. Lequeux (1994) has argued for possible H_2 toward the AZV 456 line of sight, and we noted in § 1 that there is an *IRAS* extended source toward this same direction. Let us assume that the gas-to-dust ratio toward AZV 456 equals the

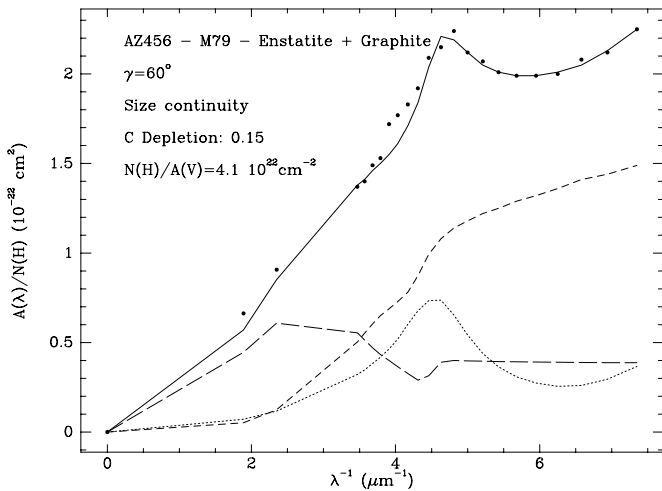


FIG. 13.—The AZV 456 extinction curve, assuming that the gas-to-dust ratio equals the $N(\text{H I})/A(V)$ ratio typical of the SMC, that of AZV 398. Dust parameters for the calculated solid line are given in Table 8. The line styles are dotted = graphite, long-dashed = silicate cylinders, and short-dashed = silicate spheres.

$N(\text{H I})/A(V)$ ratio shown by AZV 398 [i.e., a factor of about 6 higher than the observed $N(\text{H I})/A(V)$ ratio for AZV 456]. For the cylindrical grains, we take one of the grain populations that fits the polarization (Fig. 12), with a correspondingly lower Si/H abundance. The resultant extinction fit is shown in Figure 13. Note that the “bluer” bump of AZV 456 is now evident in Figure 13. The cylinders use a relatively large amount (80%) of the available Si and provide a sizable contribution to the extinction. The total Si used is about 50% more than the amount available. Our purpose here is not to opt for a particular fit, given the uncertain gas-to-dust ratio toward AZV 456, but only to show that it may be possible to fit the extinction toward this star if we assume a higher gas-to-dust ratio in its line of sight.

As a matter of fact, given that amorphous carbon (and silicates) explains so well the typical SMC extinction (§ 5.3.1), it is quite reasonable to expect this component to be present toward AZV 456 as well. The inclusion of amorphous carbon in a model will lower the amount of Si needed, since this unpolarizing, carbon component will provide some of the needed extinction as well as lower the $P(V)/A(V)$ ratio. Additionally, the best fits to the polarization of AZV 456 actually do use a small amount of Si (Table 7). The inclusion of amorphous carbon implies, of course, a larger number of free parameters. However, we have used the same size distribution for amorphous carbon obtained from the AZV 398 extinction fits and verified that indeed the overall extinction toward AZV 456 may be obtained.

6. DISCUSSION

6.1. SMC Interstellar Polarization and Extinction Data: What Do They Mean?

We now wish to discuss the data presented on the sample of stars in the SMC for which we have available both extinction curves and and/or wavelength-dependent polarization data.

Our extinction data suggest a correlation between the FUV curvature and the linear portion of the extinction curve (§ 4.2). The stars for which the FUV contribution is

more important, AZV 211 and AZV 398, do not show the bump, so the FUV curvature cannot be attributed to the same grains producing the bump. Furthermore, these two stars show λ_{max} smaller than the Galactic average. Other SMC stars also present small λ_{max} values (Table 3, col. [2]). Of the two stars in the SMC that have larger λ_{max} values, similar to those for the Galaxy, the one with the best signal-to-noise ratio, AZV 456, has a well-determined extinction curve (Prévoit et al. 1984; § 4.1). This star does show the bump, and its λ_{max} value indicates that it also is characterized by grains larger than those found for the other sight lines in the SMC. It is also of interest to note that from observations in our Galaxy, the bump is usually not polarized (Clayton et al. 1992; Anderson et al. 1997), so that the grains producing the bump are either spherical or not aligned.

It is tempting to conclude that the bump in the SMC would be present only along lines of sight characterized by large λ_{max} . This conclusion might be tenuous, since stars with both polarization and extinction curves reliably determined are very few in the SMC and there is only one known line of sight that shows the bump. However, it is rather remarkable that AZV 456 has an extinction curve similar to that for the Galaxy (Prévoit et al. 1984; § 4.1) and a λ_{max} value similar to the Galactic average (§ 3.1). All of the remaining stars in the sample of about 20 stars of Bouchet et al. (1985) and Fitzpatrick (1985b) show a gas-to-dust ratio $[N(\text{H I})/A(V)]$ roughly 10 times the Galactic average. The three stars in the sample of Prévoit et al. (1984), which have this high gas-to-dust ratio, do not show the bump. In addition, in our sample of stars, those that do not show the bump show small λ_{max} values. Extending the arguments of Fitzpatrick (1989) to include polarization data, we may say that, if the high gas-to-dust ratios are produced by conditions that also give rise to the typical SMC extinction law and small λ_{max} values, then our polarization measurements, as well as the extinction law of Prévoit et al. (1984), may indeed represent the typical extinction and polarization properties of the dust in the SMC.

The λ_{max} results from our polarization data are important in order to improve the constraints on dust models for the SMC and as a test for inferences based solely on extinction data. Bouchet et al. (1985) point out that the value of R they have determined for the SMC, slightly smaller than the Galactic value, might suggest that the graphite grains would play a smaller role in the visible/IR. According to them, the size distribution of silicate grains, in the context of the MRN model, would then have to be shifted toward larger grains. Our fits to the observations show that the opposite is actually true, λ_{max} is, in general, smaller than in the Galaxy. While it might be expected that λ_{max} would depend on how the alignment mechanism works as a function of size, studies of the correlation between extinction and polarization (Serkowski et al. 1975; Whittet & van Breda 1978; Clayton & Mathis 1988; § 3.2) for the Galaxy for several types of sight lines suggest that the populations producing extinction and polarization would seem to be affected similarly by the environment and that λ_{max} variations originate mainly from differences in the size distributions rather than variations in the alignment of particles (Clayton & Mathis 1988).

The λ_{max} results can be interpreted in terms of the dust grain sizes. Values of λ_{max} close to $0.55 \mu\text{m}$ indicate that the grains toward AZV 456 have average sizes close to those in

the Galactic diffuse ISM, although with a narrower size distribution. Inspection of the line of sight to AZV 456 using the catalog of SMC *IRAS* sources of Schwering & Israel (1989) shows that there is an extended IR source toward that object. This line of sight then indeed might not represent the typical line of sight through the diffuse ISM in the SMC, as discussed earlier in this section.

The lines of sight with smaller λ_{\max} would evidence smaller average grain sizes. They are associated with no bump in their UV extinction curves, that is, with the extinction law that is considered typical of the SMC (Prévot et al. 1984). The correlation between the FUV curvature and the linear part of the extinction curve, suggested by the data (§ 4.2), indicate smaller average grain sizes producing the typical SMC extinction. The smaller average grain sizes inferred from our polarization data and model fits strengthen this interpretation.

6.2. SMC Environment and Dust Models

As outlined in § 1, the SMC is a valuable laboratory for studying several aspects of the evolution of the dust content of the ISM in galaxies (Westerlund 1989, 1990). The UV bump in the Galactic extinction curve is thought to be produced by carbon (graphite) grains. Consequently, the lack of the bump in the SMC extinction curve is associated usually with a small quantity of carbon grains. However, there is no evidence for a carbon deficiency in the ISM of the SMC. Despite the comparison between stellar dust injection and depletion by star formation and shocks in the interstellar medium, many of the grains containing carbon are thought to come from carbon stars (e.g., Gehrz 1989). The relative number of carbon stars to normal stars in the post-main-sequence stages of stellar evolution is actually greater in the SMC than in the Milky Way (Lequeux 1988 and references therein). Also, the C/Si ratio seems to be comparable to the Galactic one (Dufton et al. 1990; see § 3). On the other hand, it has been argued that amorphous carbon grains are a more plausible interstellar component than graphite (Bussoletti, Colangeli, & Orofino 1988 and references therein). Studies of interplanetary dust show that graphite is present only in trace amounts (Nuth 1985). Amorphous carbon has been detected around R CrB stars also (Hecht et al. 1984).

The typical SMC extinction curve, shown by AZV 398, can be best fitted with amorphous carbon grains rather than with graphite grains (§ 5.3.1). Moreover, with graphite, the required Si abundance is somewhat greater than that available in the SMC. Support for an amorphous carbon component to the AZV 398 extinction is provided additionally by the star HD 89353 (= HR 4049), whose extinction curve has no bump but a high, quasi-linear rise into the UV produced by grains in a circumstellar envelope (Buss, Lamers, & Snow 1989). Among the stars in the Galaxy, it is one of the poorest in metals and one of the richest in hydrogen and carbon. Blanco, Fonti, & Orofino (1995) were able to fit its extinction using optical constants of amorphous carbon rich in H. On the other hand, Mennella et al. (1995) show that initially H-rich amorphous carbon grains progressively lose their H as annealing occurs. The extinction bump varies in position and strength according to the annealing temperature. How could H-rich amorphous carbon survive in the SMC ISM, an environment with a high-UV interstellar radiation field (ISRF)? What is the role of the ISM metallicity in grain evolution? Jenniskens et al.

(1993) suggested that an icy mantle formed in molecular clouds can be transformed into an organic residue due to action of the FUV radiation, and that a prolonged exposure to this radiation can lead to the formation of amorphous aromatic carbon.

In the line of sight to AZV 456, which seems to have larger grains, there is an IR emission associated with cold dust. This can be considered, therefore, as a region with density enhancement, similar to the Galactic molecular clouds. The small gas-to-dust ratio toward this region also could be an indication of the presence of molecular hydrogen (Lequeux 1994). If this indeed happens, we can expect that the enhanced density will lead to the accretion of smaller grains onto the larger ones. This will increase the average size and reduce the width of the grain size distribution, as seen in the AZV 456 results. If we believe that (part of) the line of sight to AZV 456 really is characterized by higher densities, then the grains could be shielded from the strong ISRF, and the carriers of the 2175 Å bump could survive. Recently, Andersson & Wannier (1995) found a Galactic molecular cloud whose dust is characterized by normal values of λ_{\max} and large K .

It has been suggested (Sorrel 1990) that carbon is transformed into graphite in the ISM by an annealing process caused by the ISRF. In that case, the SMC would be a privileged site for graphite formation because the ISRF is greater there than in the Galaxy (Lequeux 1989). But that does not seem to be the case, since the UV bump is not observed generally.

Actually, the higher ISRF in the SMC might have a bearing on the absence of a UV bump in the typical SMC extinction curve. Leene & Cox (1987) found a correlation between the 60 $\mu\text{m}/100 \mu\text{m}$ brightness ratio, a measure of dust temperature, and the height of the Galactic UV bump in the sense that the bump gets weaker when the 60 $\mu\text{m}/100 \mu\text{m}$ ratio (and presumably the ISRF) gets higher. They suggested that the particles responsible for the UV bump are very sensitive to the ISRF intensity. Jenniskens & Greenberg (1993) also found that the bump is sensitive to strong UV radiation fields from their studies of Galactic extinction curves and the environment.

We now wish to point out some implications of the SMC data and the hypothesis of polycyclic aromatic hydrocarbons (PAHs). Jenniskens, Ehrefreund, & Désert (1992) have found a correlation between the amount of FUV rise (c_4 ; § 4.1) and the CH abundance in the line of sight to several Galactic stars. Since CH is directly proportional to molecular hydrogen, they suggested that the carrier of the FUV rise coexists with the medium containing H_2 . They also suggested that the FUV rise is associated with the PAHs. As we have seen, AZV 456 is related to an IR extended source, and its smaller gas-to-dust ratio suggests the presence of H_2 . However, it is precisely AZV 456 that shows a small value of c_4 (Table 6 and Fig. 7).

A related question concerns the PAH hypothesis and the IR emission of the SMC. Sauvage, Thuan, & Vigroux (1990) presented the colors of the *IRAS* IR emission of the LMC and SMC, and correlated them with the age and metallicity of the underlying stellar populations. Lequeux (1989) has reviewed nicely these and other IR data and their implications for the interstellar dust in the Magellanic Clouds. The integrated 12 μm emission of the SMC (Rice et al. 1988; Schwering 1988) is especially low among irregular galaxies, suggesting that the PAHs, believed to be responsible for

such emission, are less abundant, perhaps having been destroyed by photodissociation by the more abundant FUV photons. This could be due to the larger ISRF in the SMC. The *IRAS* color-color diagrams suggest that the SMC may be rich in small ($\lesssim 0.05 \mu\text{m}$) grains responsible for the extinction shortward of 2000 Å. While the SMC extinction and the polarization data we provide herein support the abundance of small grains, the steep FUV extinction and low 12 μm emission seem to rule out the PAHs as suggested by Désert, Boulanger, & Puget (1990).

7. SUMMARY

In order to study the grains in the SMC, which has an extinction curve very different from that for the Galaxy, we have obtained the first wavelength-dependent polarization measurements for stars in the SMC. From an analysis of these and the extinction curves, for which we present some new *IUE* data, for a small sample of stars we reach the following conclusions:

1. The wavelength of maximum polarization, λ_{max} , determined from a fit of the Serkowski curve to the new polarization data, is generally smaller than in the Galaxy.

2. For AZV 456, the single, well-studied case that shows the extinction bump at 2175 Å, λ_{max} is typical of that in the Galaxy; at the same time, the bump for this star is shifted to the blue, as compared with the Galaxy, and its polarization curve is narrower.

3. The FUV curvature and the linear component of the extinction curve increase simultaneously for stars with small λ_{max} .

We attempt to fit both the extinction and the polarization data for stars in the SMC by varying the mean size and the

size distribution of the grains within the framework of the MRN model and introducing the notion of volume continuity. Our results are as follows:

1. The AZV 398 (i.e., the typical SMC) extinction curve is best fitted using, in addition to silicates, amorphous carbon instead of graphite. The polarization data and the polarization and extinction fits indicate smaller grains in the SMC as compared with the Galaxy. Contrary to earlier belief, silicate alone cannot provide the amount of extinction observed toward the SMC, despite its providing an approximately correct wavelength dependence.

2. It appears that for AZV 456, there may be a contribution, not yet accounted for, of H_2 to the actual ratio, $N(\text{H})/A(V)$.

Our results indicate that the typical line of sight in the SMC is characterized by grains smaller and of a different type on the average than those in the Galaxy. This may be further evidence that the dust grains have formed and evolved somewhat differently and/or at a different rate in the SMC environment than they have in the Galaxy.

This work has been supported by NASA grant NAG 5-1463. It also has been partially supported by FAPESP (C. V. R.: 89/3091-6; A. M. M.: 89/1670-9, 92/3345-0, and 94/0033-3) and CNPq (A. M. M.: 301558/79-5). A. M. M. and C. V. R. would like to acknowledge the hospitality provided by A. Code, Space Astronomy Laboratory and Astronomy Department, University of Wisconsin, where this research was partly done. We would like to thank the referee, Peter Martin, for his valuable criticism that helped improve the paper.

REFERENCES

- Anders, E., & Grevesse, N. 1989, *Geochim. Cosmochim. Acta*, 53, 197
 Anderson, C. M., et al. 1997, *ApJ*, submitted
 Andersson, B.-G., & Wannier, P. G. 1995, *ApJ*, 443, L49
 Ardeberg, A., Brunet, J. P., Maurice, E., & Prévot, L. 1972, *A&AS*, 6, 249
 Azzopardi, M., & Vigneau, J. 1982, *A&AS*, 50, 291 (AZV82)
 Bessel, M. S. 1991, *A&A*, 242, L17
 Blanco, A., Fonti, S., & Orofino, V. 1995, *ApJ*, 448, 339
 Boggess, A., et al. 1978a, *Nature*, 275, 372
 ———. 1978b, *Nature*, 275, 377
 Bohlin, R. C., & Grillmair, C. J. 1988a, *ApJS*, 66, 209
 ———. 1988b, *ApJS*, 68, 487
 Bohlin, R. C., Savage, B. D., & Drake, J. F. 1978, *ApJ*, 224, 132
 Bouchet, P., Lequeux, J., Maurice, E., Prévot, L., & Prévot-Burnichon, M. L. 1985, *A&A*, 149, 330
 Bromage, G. E., & Nandy, K. 1983, *MNRAS*, 204, 29P
 Brunet, J. P. 1975, *A&A*, 43, 345
 Burton, W. B., Deul, E. R., Walker, H. J., & Jongeneelen, A. A. W. 1986, in *Light on Dark Matter*, ed. F. P. Israel (Dordrecht: Reidel), 357
 Buss, R. H., Jr., Lamers, H. J. G. L. M., & Snow, T. P., Jr. 1989, *ApJ*, 347, 977
 Bussoletti, E., Colangeli, L., & Orofino, V. 1988, in *Experiments Cosmic Dust Analogues*, ed. E. Bussoletti, C. Fusco, & G. Longo (Dordrecht: Kluwer), 63
 Cardelli, J. A., & Clayton, G. C. 1991, *AJ*, 101, 1021
 Cardelli, J. A., Clayton, G. C., & Mathis, J. S. 1989, *ApJ*, 345, 245
 Cardelli, J. A., & Savage, B. D. 1988, *ApJ*, 325, 864
 Casey, S. 1991, *ApJ*, 371, 183
 Chini, R., & Krügel, E. 1983, *A&A*, 117, 289
 Chlewicki, G., & Greenberg, J. M. 1990, *ApJ*, 365, 230
 Clarke, D., & Stewart, B. G. 1986, *Vistas Astron.*, 29, 27
 Clayton, G. C., et al. 1992, *ApJ*, 385, L53
 Clayton, G. C., Green, J., Wolff, M. J., Zellner, N. E. B., Code, A. D., & Davidsen, A. F. 1997, *ApJ*, in press
 Clayton, G. C., & Martin, P. G. 1985, *ApJ*, 288, 558
 Clayton, G. C., Martin, P. G., & Thomson, I. 1983, *ApJ*, 265, 194
 Clayton, G. C., & Mathis, J. S. 1988, *ApJ*, 327, 911
 Clayton, G. C., Wolff, M., Allen, R. G., & Lupie, O. L. 1995, *ApJ*, 445, 947
 Codina-Landaberry, S., & Magalhães, A. M. 1976, *A&A*, 49, 407
 Coyne, G. V., Gehrels, T., & Serkowski, K. 1974, *AJ*, 79, 581
 Crampton, D., & Greasley, J. 1982, *PASP*, 94, 31
 Désert, F.-X., Boulanger, F., & Puget, J. L. 1990, *A&A*, 237, 215
 Draine, B. T., & Lee, H. M. 1984, *ApJ*, 285, 89
 Draine, B. T., & Malhotra, S. 1993, *ApJ*, 414, 632
 Dufton, P. L., Fitzsimmons, A., & Howarth, I. D. 1990, *ApJ*, 362, L59
 Duley, W. W. 1984, *ApJ*, 287, 694
 Fitzgerald, M. P. 1970, *A&A*, 4, 234
 Fitzpatrick, E. L. 1985a, *ApJ*, 299, 219
 ———. 1985b, *ApJS*, 59, 77
 ———. 1986, *AJ*, 92, 1068
 ———. 1989, in *IAU Symp. 135, Interstellar Dust*, ed. L. J. Allamandola & A. G. G. M. Tielens (Dordrecht: Kluwer), 37
 Fitzpatrick, E. L., & Massa, D. 1986, *ApJ*, 307, 286
 ———. 1988, *ApJ*, 328, 734
 ———. 1990, *ApJS*, 72, 163
 Frecker, J., & Serkowski, K. 1976, *Appl. Opt.*, 15, 605
 Garmany, C. D., Conti, P. S., & Massey, P. 1987, *AJ*, 93, 1070
 Gehr, R. D. 1989, in *IAU Symp. 135, Interstellar Dust*, ed. L. J. Allamandola & A. G. G. M. Tielens (Dordrecht: Kluwer), 445
 Greenberg, J. M., & Chlewicki, G. 1983, *ApJ*, 272, 563
 Hecht, J., Holm, A. V., Donn, B., & Wu, C. C. 1984, *ApJ*, 280, 228
 Huffman, D. R., & Stapp, J. L. 1971, *Nature Phys. Sci.*, 229, 45
 Humphreys, R. M. 1983, *ApJ*, 265, 176
 Jenniskens, P., Baratta, G. A., Kouchi, A., de Groot, M. S., Greenberg, J. M., & Strazzulla, G. 1993, *A&A*, 273, 583
 Jenniskens, P., Ehrefreund, P., & Désert, F.-X. 1992, *A&A*, 265, L1
 Jenniskens, P., & Greenberg, J. M. 1993, *A&A*, 274, 439
 Jones, R. V., & Spitzer, L., Jr. 1967, *ApJ*, 147, 943
 Kim, S.-H., & Martin, P. G. 1994, *ApJ*, 431, 783
 ———. 1995, *ApJ*, 444, 293
 ———. 1996, *ApJ*, 462, 296
 Kim, S.-H., Martin, P. G., & Hendry, P. D. 1994, *ApJ*, 422, 164
 Kondo, Y. 1987, *Exploring the Universe with the IUE Satellite* (Dordrecht: Kluwer)
 Koorneef, J. 1982, *A&A*, 107, 247
 Koorneef, J., & Code, A. D. 1981, *ApJ*, 247, 860
 Leene, A., & Cox, P. 1987, *A&A*, 174, L1

- Lequeux, J. 1988, in *Dust in the Universe*, ed. E. M. Bailey & D. A. Williams (Cambridge: Cambridge Univ. Press), 449
- . 1989, in *Recent Developments of Magellanic Cloud Research*, ed. K. S. de Boer, F. Spite, & G. Stasinska (Paris: Obs. Paris), 119
- . 1994, *A&A*, 287, 368
- Lequeux, J., Le Bourlot, J., Pineau des Forêts, G., Roueff, E., Boulanger, F., & Rubio, M. 1994, *A&A*, 292, 371
- Lequeux, J., Maurice, E., Prévot, L., Prévot-Burnichon, M. L., & Rocca-Volmerange, B. 1984, *A&A*, 113, L5
- Maccioni, A., & Perinotto, M. 1994, *A&A*, 284, 241
- Magalhães, A. M., Benedetti, E., & Roland, E. H. 1984, *PASP*, 96, 383
- Magalhães, A. M., Loiseau, N., Rodrigues, C. V., & Piirola, V. 1990, in *IAU Symp. 140, Galactic and Intergalactic Magnetic Fields*, ed. R. Beck, P. P. Kronberg, & R. Wielebinski (Dordrecht: Kluwer), 255
- Magalhães, A. M., Rodrigues, C. V., Margoniner, V. E., Pereyra, A., & Heathcote, S. 1996, in *ASP Conf. Ser. 97, Polarimetry of the Interstellar Medium*, ed. W. G. Roberge & D. C. B. Whittet (San Francisco: ASP), in press
- Martin, N., Maurice, E., & Lequeux, J. 1989, *A&A*, 215, 219
- Mathewson, D. S., & Ford, V. L. 1970, *AJ*, 75, 778
- Mathis, J. S. 1979, *ApJ*, 232, 747
- . 1986, *ApJ*, 308, 281
- . 1994, *ApJ*, 422, 176
- Mathis, J. S., Rumpl, W., & Nordsieck, K. H. 1977, *ApJ*, 217, 425 (MRN)
- McNamara, D. H., & Feltz, K. H. 1980, *PASP*, 92, 587
- Mennella, V., Colangeli, L., Bussoletti, E., Monaco, G., Palumbo, P., & Rotundi, A. 1995, *ApJS*, 100, 149
- Nandy, K., Morgan, D. H., Willis, A. J., Wilson, R., & Gondhalekar, P. M. 1981, *MNRAS*, 196, 955
- Nuth, J. A. 1985, *Nature*, 318, 166
- Pagel, B. E. J. 1993, in *News Aspects of Magellanic Cloud Research*, ed. B. Baschek, G. Klare, & J. Lequeux (Berlin: Springer), 330
- Pei, Y. C. 1992, *ApJ*, 395, 130
- Prévot, M. L., Lequeux, J., Maurice, E., Prévot, L., & Rocca-Volmerange, B. 1984, *A&A*, 132, 389
- Rice, W., Lonsdale, C. J., Soifer, B. T., Neugebauer, G., Kaplan, E. L., Lloyd, L. A., de Jong, T., & Habing, H. J. 1988, *ApJS*, 68, 91
- Rodrigues, C. V. 1992, MSc thesis, Instituto Astronômico e Geofísico, USP
- Sanduleak, N. 1968, *AJ*, 73, 246
- . 1969, *AJ*, 74, 877
- Sauvage, M., Thuan, T. X., & Vigroux, L. 1990, *A&A*, 237, 296
- Schmidt, Th. 1976, *A&AS*, 24, 357
- Schwering, P. B. W. 1988, Ph.D. thesis, Univ. Leiden
- Schwering, P. B. W., & Israel, F. P. 1989, *A&AS*, 79, 79
- Seaton, M. J. 1979, *MNRAS*, 187, 73P
- Serkowski, K. 1973, *IAU Symp. 52, Interstellar Dust and Related Topics*, ed. J. M. Greenberg & H. C. van der Hulst (Dordrecht: Reidel), 145
- Serkowski, K., Mathewson, D. S., & Ford, V. L. 1975, *ApJ*, 196, 261
- Sorrell, W. H. 1990, *MNRAS*, 243, 570
- Stahl, O., Buzzoni, B., Kraus, G., Schwarz, H., Metz, K., & Roth, M. 1986, *Messenger*, 46, 23
- Westerlund, B. E. 1989, in *Recent Developments of Magellanic Cloud Research*, ed. K. S. de Boer, F. Spite, & G. Stasinska (Paris: Obs. Paris), 159
- . 1990, *A&A Rev.*, 2, 29
- Wheeler, J. C., Sneden, C., & Truran, J. W., Jr. 1989, *ARA&A*, 27, 279
- Whittet, D. C. B., Martin, P., Hough, J., Rouse, M., Bailey, J., & Axon, D. 1992, *ApJ*, 386, 562
- Whittet, D. C. B., & van Breda, I. G. 1978, *A&A*, 66, 57
- Wilking, B. A., Lebofsky, M. J., Martin, P. G., Rieke, G. H., & Kemp, J. C. 1980, *ApJ* 235, 905
- Wilking, B. A., Lebofsky, M. J., & Rieke, G. H. 1982, *AJ*, 87, 905
- Wolf, M. J., Clayton, G. C., Martin, P. G., & Schulte-Ladbeck, R. E. 1994, *ApJ*, 423, 412
- Xu, C., & Helou, G. 1994, *ApJ*, 426, 109